PEPIN R. O. (1980) Rare gases in the past and present solar wind. In *Prof. Conf. Ancient Sun* (eds. R. O. Pepin, J. A. Eddy and R. B. Morrill), pp. 411–421. Pergamon Press, New York.

WIELER R., BAUR H. AND SIGNER P. (1986) Noble gases from solar energetic particles revealed by closed system stepwise etching of lunar soil minerals. *Geochim Cosmochim. Acta* **50**, 1997–2017.

A new titanium-bearing calcium aluminosilicate phase: I. Meteoritic occurrences and formation in synthetic systems

JULIE M. PAQUE[1], JOHN R. BECKETT[2], DAVID J. BARBER[3]* AND EDWARD M. STOLPER[2]

[1]SETI Institute, NASA-Ames Research Center, MS 244-11, Moffett Field, California 94035-1000, USA
[2]Division of Geological and Planetary Sciences, California Institute of Technology, Pasadena, California 91125, USA
[3]Physics Department, University of Essex, Colchester, Essex, CO4 3SQ, U. K.
*Current address: Physics Department, The Hong Kong University of Science and Technology, Clear Water Bay, Kowloon, Hong Kong

(Received 1993 September 28; accepted in revised form 1994 May 3)

Abstract–A new titanium-bearing calcium aluminosilicate mineral has been identified in coarse-grained calcium-aluminum-rich inclusions (CAIs) from carbonaceous chondrites. The formula for this phase, which we have temporarily termed "UNK," is $Ca_3Ti(Al,Ti)_2(Si,Al)_3O_{14}$, and it is present in at least 8 of the 20 coarse-grained CAIs from the Allende CV3 chondrite examined as part of this project. The phase occurs in Types A and B1 inclusions as small tabular crystals oriented along two mutually perpendicular planes in melilite.

UNK crystallizes from melts in dynamic crystallization experiments conducted in air from four bulk compositions modeled after Types A, B1, B2 and C inclusions. Cooling rates resulting in crystallization of UNK ranged from 0.5 to 200 °C/h from maximum (initial) temperatures of 1375 to 1580 °C. Only below 1190 °C does UNK itself begin to crystallize. To first order, the presence or absence of UNK from individual experiments can be understood in terms of the compositions of residual melts and nucleation probabilities.

Compositions of synthetic and meteoritic UNK are very similar in terms of major oxides, differing only in the small amounts of trivalent Ti (7–13% of total Ti) in meteoritic samples. UNK crystallized from the Type A analog is similar texturally to that found in CAIs, although glass, which is typically associated with synthetic UNK, is not observed in meteoritic occurrences. A low Ti end-member of UNK ("Si-UNK") with a composition near that of $Ca_3Al_2Si_4O_{14}$ was produced in a few samples from the Type B1 analog. This phase has not been found in the meteoritic inclusions.

INTRODUCTION

Calcium-aluminum-rich inclusions (CAIs) from carbonaceous chondrites have been studied intensely to determine physical conditions during the early history of our Solar System (MacPherson *et al.*, 1988; and references therein). Coarse-grained CAIs, those that can be studied by standard petrographic techniques, are host to minerals formed at different stages in the evolution of the inclusions so that each mineral constrains specific aspects of the history of CAIs. This is the first in a series of three papers dealing with a new mineral, which we term "UNK" following Paque *et al.* (1986). This work describes the characteristics of meteoritic UNK from coarse-grained inclusions in the Allende meteorite, the conditions under which it can be produced in dynamic crystallization experiments, and the relevance of melting to the origin of meteoritic UNK. The second paper deals with the crystallography and crystal chemistry of synthetic UNK crystallized during a cooling rate experiment on a CAI bulk composition and hypotheses relating to its formation and significance to the early history of the Solar System (Barber *et al.*, 1994). In the third paper, the space group of UNK is constrained using crystals from a mixer furnace slag (Barber and Agrell, 1994).

UNK, with the chemical formula $Ca_3Ti(Al,Ti)_2(Si,Al)_3O_{14}$ (see Barber *et al.*, 1994), was first noted in synthetic slag samples by Agrell (1945) and in a CAI from the meteorite Essebi by El Goresy *et al.* (1984). The phase has also been noted in synthetic samples produced in several experimental studies of CAIs (Paque and Stolper, 1984; Paque *et al.*, 1986; Beckett and Stolper, 1994; this study). More recently, Floss *et al.* (1992) described an unusually Ti-rich, Al-poor phase probably related to UNK from an Allende Type A inclusion.

ANALYTICAL PROCEDURES

Phases were identified and textures observed by backscattered and secondary electron imaging on a JEOL 733 microprobe at the Smithsonian Astrophysical Observatory. Chemical analyses were also performed on this microprobe. Accelerating voltage was 15 kV and sample current 15 to 30 nA as measured on a Faraday cup placed in the path of the beam. Counting times for each element ranged from 15 to 30 s for the majority of analyses, and recalculation of the raw data followed the method of Albee and Ray (1970). A glass similar in composition to a Ti-fassaite was used as an internal standard.

EXPERIMENTAL PROCEDURES

Starting Materials

CAIs are classified according to textures and relative amounts of major phases (*e.g.*, MacPherson *et al.*, 1988). Type A inclusions are composed mainly of melilite, with minor amounts of spinel, hibonite, perovskite, and Ti-fassaite. They can be subdivided into compact Type A inclusions (CTA) characterized by rounded shapes and axiolitic intergrowths of melilite, and fluffy Type A inclusions (FTA) with irregular shapes. Type B2 inclusions have sub-equal amounts of melilite, anorthite, pyroxene, and spinel, while Type B1 inclusions are characterized by a melilite-rich mantle surrounding a core that is petrographically similar to Type B2s. Type C inclusions are similar to Type B2s but are unusually rich in anorthite and poor in melilite. Compact Type As and Types B and C inclusions are generally thought to have crystallized from partially molten droplets. The role, if any, of melts in the evolution of fluffy Type As is still controversial (*e.g.*, MacPherson *et al.*, 1988). We synthesized four bulk compositions representing the different types of Allende CAIs as part of a larger study on the crystallization properties of CAIs. The compositions represent melilite-rich Type A ("98": SiO_2, 25.8; TiO_2, 1.51; Al_2O_3, 32.6; MgO, 6.65; CaO, 33.7), pyroxene-rich Type B1 ("CAI": SiO_2, 31.4; TiO_2, 1.13; Al_2O_3, 28.3; MgO, 9.9; CaO, 29.1) and Type B2("B2C": SiO_2, 35.7; TiO_2, 1.39; Al_2O_3, 27.1; MgO, 12.9; CaO, 22.4) and anorthite-rich Type C ("TCAN": SiO_2, 38.8; TiO_2, 1.31; Al_2O_3, 29.0; MgO, 5.77; CaO, 24.9) inclusions.

Starting materials were prepared by mixing high purity oxides and carbonates under ethanol in an automated agate mortar for 5 h or more, followed by decarbonation at 1000 °C, melting in air for one day at either 1525 °C or 1550 °C, and quenching in deionized water after removing the crucible

through the top of the furnace. Further details on preparation of the starting materials and the experimental techniques can be found in Stolper and Paque (1986).

Crystallization Experiments

A summary of isothermal crystallization sequences for the bulk compositions used in this study can be found in Paque and Stolper (1984) along with preliminary results on the controlled cooling experiments. Crystallization behavior of the CAI bulk composition has also been studied by Stolper (1982), MacPherson *et al.* (1984), Stolper and Paque (1986) and Beckett *et al.* (1990). UNK was synthesized for this study in dynamic crystallization experiments performed in air in a vertical tube Deltech VT-31 furnace. The sample temperature was monitored with a $Pt/Pt_{10}Rh$ (Type S) thermocouple calibrated against the melting points of Au (1064 °C) and Pd (1554 °C) and placed in the hot spot adjacent to the samples. In each experiment, several powdered samples of the synthetic material were suspended in the hot spot using Pt loops. Samples were held for 3 h at the maximum temperature of the experiment (T_{max}), then cooled at a controlled, approximately linear rate. Individual samples were quenched in deionized water at various temperatures along the cooling path in order to determine the temperature of appearance for individual phases and the liquid line of descent.

RESULTS

Meteoritic Occurrence of UNK

A survey of 20 coarse-grained Allende CAIs (four compact Type As, two fluffy Type As, eleven B1s, and three B2s) was conducted to determine the extent to which UNK occurs in natural materials and the variability in its composition and nature of occurrence. The search was carried out using a JEOL 733 electron microprobe. Initially, the sample was scanned using backscattered electron (BSE) imaging to locate potential grains of UNK, which has a lower BSE albedo than perovskite, but higher than melilite, anorthite, spinel, and all but the most Ti-rich fassaites (>15 wt% TiO_2) due to its high mean atomic number (Z). Energy dispersive spectroscopy (EDS) was then used to confirm the identification of UNK. Final analyses were made by wavelength dispersive spectroscopic (WDS) analysis. UNK is a minor constituent of approximately half of the Type A and Type B1 inclusions examined. It was positively identified in one CTA (4691), one FTA (A-WP1), and six Type B1s (3529-30, 3529-33, 3529-41, 3655A, 3658, 3682). No likely candidates for UNK grains were observed in CTAs 3643 or 3898, FTA 3529-46, B1s 3529Y, 3529Z, 3529-21 or 3529-31, or B2s All-201, RB-83-1 or 3529-32. For two inclusions, CTA 3529-45 and the Type B1 3732-1, the grain size (<1 μm) of phases tentatively identified as UNK was so small that it was not possible to demonstrate conclusively that the grains were UNK. In the Type A CAIs, UNK can be found in melilite throughout the inclusion. In Type B1s, UNK occurs only in the melilite mantle and is most commonly found in regions close to the rim (*i.e.*, the outer quarter of the melilite-rich mantle) of the inclusion. UNK was not observed in any of the Type B2 inclusions surveyed, although the sample set included only three inclusions. Type C inclusions were not studied as part of this project.

Petrography of Meteoritic UNK—All of the meteoritic UNK crystals are enclosed in melilite. The crystals are typically tabular in thin section (Fig. 1a), although occasionally they occur as anhedral crystals embedded in melilite (Fig. 1b). Crystals of UNK are often found at the intersection of two perpendicular planes of cleavage ({001} and {110}; *cf.* Deer *et al.*, 1992) in melilite. There are usually several to many grains within different melilite crystals in a given CAI, all less than 10 μm in maximum dimension. They are colorless in plane polarized light, and the larger crystals display third order interference colors under crossed nicols consistent with indices of refraction measured by Barber and Agrell (1994) on synthetic crystals of UNK from a mixer furnace slag. Extinction is parallel to the length of the crystals, and the reflectivity is slightly higher than that of fassaite.

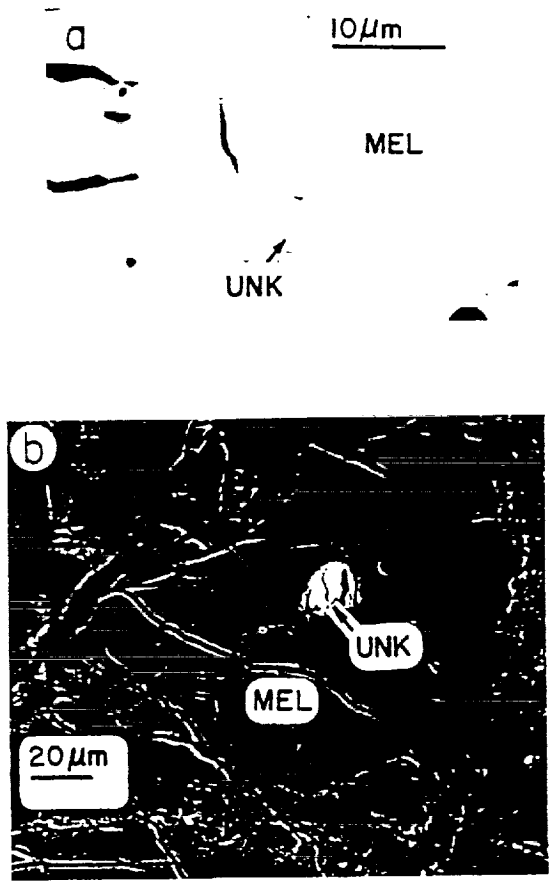

FIG. 1. Backscattered electron (BSE) images of UNK from Allende Type B1 inclusions. (a) NMNH 3682. Tabular crystals of UNK are oriented with long direction parallel to the c-axis in the melilite (MEL). (b) NMNH 3529-41. This is the largest meteoritic grain of UNK found to date.

Chemistry of Meteoritic UNK and Coexisting Melilite—Table 1 shows representative analyses of UNK from meteoritic samples. The phase contains subequal amounts of CaO (29–32 wt%), SiO_2 (24–28%), and TiO_2 (20–27%) with less Al_2O_3 (16–20%) and very low MgO (<1%). Calcium consistently represents one-third of the cations present, and deviations in analyses from Ca + Mg = 3.0 cations in a formula unit based on 9.0 cations can be attributed to contamination of the analyses by surrounding melilite. Figure 2a shows cations of Si *vs.* cations of Ti for UNK analyses from Type B1 inclusions with 3.00 ± 0.05 cations of Ca in a formula unit based on 14 oxygens. All of the analyses plot close to, but slightly above, the Si + Ti = 4.0 line, probably a consequence of assuming that all Ti is tetravalent. If a stoichiometry of 9 cations and 14 oxygens is assumed and the valence state of Ti allowed to float, then analyses are consistent with the presence of small amounts, 7–13%, of trivalent Ti. Due to the limited spatial resolution of the electron microprobe, zoning can be characterized only in the largest crystals in Type B1 inclusions. These are consistent with slightly higher Ti in the core relative to the rim (Fig. 3a).

In Fig. 4, compositions of meteoritic UNK are cast in terms of the three components:

$$(Ca,Mg)_3Ti_2^{4+}Al_2Si_2O_{14},\quad (Ca,Mg)_3Al_2Si_4O_{14}\ \text{and}$$

TABLE 1. Selected analyses of UNK from Allende CAIs.

Inclusion	A-WP1	4691	3655A	3529-33	3529-41	3529-30	3682	3658	Essebi*
Type	FTA	CTA	B1	B1	B1	B1	B1	B1	
SiO_2	25.7	24.0	24.8	27.3	27.0	27.6	24.0	25.4	24.6
TiO_2**	20.4	24.1	27.2	24.1	23.9	23.6	26.9	26.9	27.1
Al_2O_3	19.5	18.0	17.9	17.0	17.6	17.2	16.6	16.2	16.1
MgO	0.77	0.34	0.29	0.49	0.14	0.12	0.39	0.35	0.36
CaO	32.2	31.7	31.9	31.2	30.5	31.0	30.6	30.6	29.3
Total	98.6	98.1	102.1	100.1	99.1	99.5	98.5	99.5	97.5
				Cations based on total = 9					
Si	2.37	2.20	2.21	2.46	2.45	2.51	2.23	2.33	2.30
Ti	1.41	1.67	1.82	1.64	1.64	1.61	1.88	1.85	1.91
Al	2.11	1.95	1.88	1.81	1.88	1.84	1.82	1.75	1.78
Mg	0.11	0.05	0.04	0.06	0.02	0.02	0.05	0.05	0.05
Ca	3.17	3.12	3.05	3.02	2.97	3.01	3.04	3.02	2.94
Si + Ti	3.78	3.87	4.03	4.10	4.09	4.12	4.11	4.18	4.21

* El Goresy *et al.* (1984); the phase also contains 1.1 wt% of the rare earth elements and 0.2% each of ZrO_2 and HfO_2.
** All Ti is calculated as TiO_2.

$(Ca,Mg)_3Ti^{4+}Ti^{3+}_2Si_3O_{14}$. Each open symbol represents the average of all UNK analyses obtained from an individual CAI, corrected for melilite contamination and variable Ti^{3+}/Ti^{4+} by requiring that the formula unit have 3.00 Ca + Mg cations, 9 total cations and 14 oxygens. The meteoritic UNKs are composed mostly of $Ca_3Ti^{3+}_2Al_2Si_2O_{14}$ with lesser amounts of $(Ca,Mg)_3Al_2Si_4O_{14}$ and $Ca_3Ti^{4+}Ti^{3+}_2Si_3O_{14}$. The calculated mole fraction of $Ca_3Ti^{4+}Ti^{3+}_2Si_3O_{14}$ is sensitive to the assumed composition of co-existing melilite and the MgO wt% in the analysis, leading to uncertainties on the order of ±5 mol%. There are no obvious compositional differences among UNKs from different classes of CAIs, but all are consistent with the presence of small amounts of trivalent Ti and, therefore, growth under reducing conditions.

Melilite in CAIs is essentially a binary solid solution between the end-member components gehlenite (Ge: $Ca_2Al_2SiO_7$) and åkermanite (Ak: $Ca_2MgSi_2O_7$). When viewed in transmitted cross-polarized light, UNK crystals often appear to be surrounded by a halo of anomalously birefringent melilite relative to nearby portions of the host melilite crystal. This is borne out by measured melilite compositions at melilite-UNK contacts, which are highly variable (Ak_{12} to Ak_{66}) but generally (Fig. 5b), though not always (Fig. 5a), more magnesian than expected based on regional zoning of the melilite. The zoning profile shown in Fig. 5b is for melilite in the vicinity of the UNK crystal depicted in Fig. 1b.

Synthetic UNK

Conditions of Formation and Chemistry–UNK is an occasional constituent of run products from cooling rate experiments from all four bulk compositions under conditions summarized in Fig. 6, but absent from all isothermal experiments. Typically, several samples were run under the same conditions of initial temperature (T_{max}) and cooling rate (CR), then quenched at various temperatures. UNK was noted as being present in Fig. 6 if any of the samples produced under the stated conditions of T_{max} and CR contained the phase. To eliminate from consideration run sequences that did not include samples cooled to temperatures low

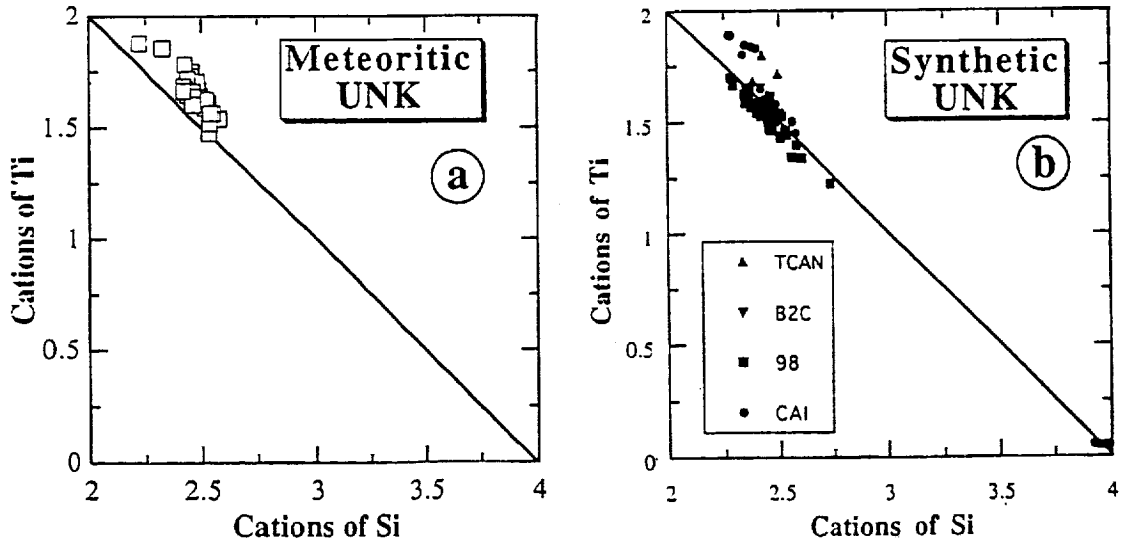

FIG. 2. Relationship between Ti and Si in UNK, based on a total of 9 cations, for all analyses with Ca = 3.00 ± 0.05 cations. The solid line indicates Si + Ti = 4.0. (a) Meteoritic Type B1 and (b) Synthetic.

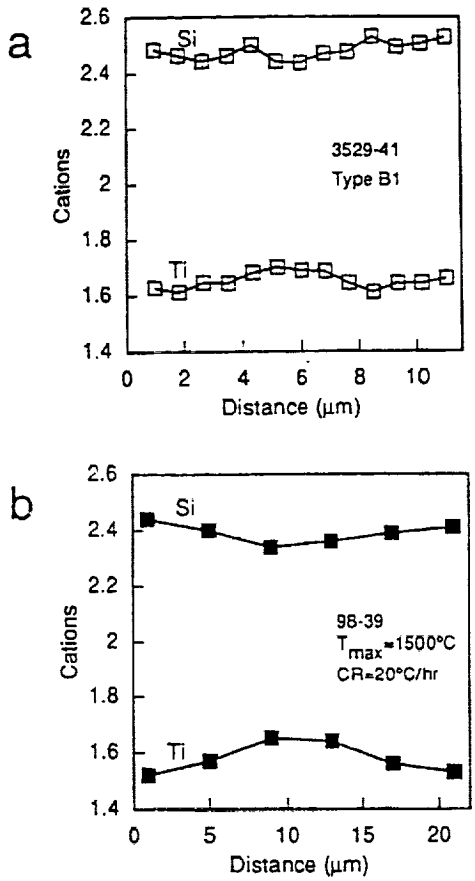

FIG. 3. Zoning pattern in UNK from (a) NMNH 3529-41, a Type B1 CAI from Allende, and (b) 98-39 (T_{max} = 1500 °C, CR = 20 °C/h). Cations are based on a sum total of 9. Traverses are in straight lines from one crystal edge through the center to the opposite edge.

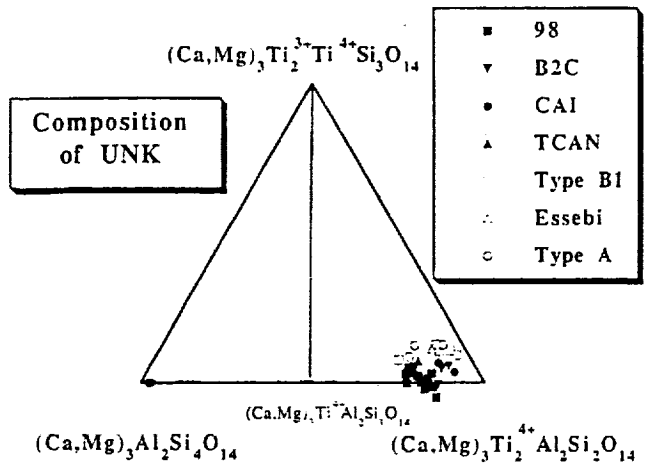

FIG. 4. Compositions in mol% of synthetic (closed symbols) and meteoritic (open symbols) UNK in terms of the three components $(Ca,Mg)_3Ti_2^{3+}Al_2Si_2O_{14}$, $(Ca,Mg)_3Al_2Si_4O_{14}$, and $(Ca,Mg)_3Ti_2^{3+}Ti^{4+}Si_3O_{14}$. Analyses of UNK were corrected for small amounts (<10 wt%) of melilite contamination such that cations of Mg + Ca = 3.00 in a formula unit based on a sum total of 9.00 cations and 14.00 oxygens. Among analyses of synthetic UNK, grains from intergrowths are not plotted because the bulk composition of the contamination was uncertain. Also, Si-UNKs were assumed to have $Ti^{3+}/Ti^{4+} = 0$ because Ti contents are too low (<1 wt% as TiO_2) to allow quantitative calculations.

enough to enter the range in which UNK was likely to crystallize, only those series of experiments extending to quench temperatures below 1100 °C are plotted. In the CAI (Fig. 6a) and B2C (Fig. 6b) bulk compositions, UNK crystallizes over a restricted range in T_{max} and CR. Only those CAI experiments cooled from T_{max} = 1375 and 1420 °C with CR ≤ 50 °C/h, and B2C experiments cooled from 1400–1500 °C with CR ≤ 20 °C/h produced UNK. UNK failed to appear in experiments at higher or lower T_{max} or at higher cooling rates. In contrast, UNK crystallization occurred over virtually all conditions examined for the 98 bulk composition (Fig. 6c). The data base for TCAN (Fig. 6d) is insufficient to characterize the crystallization behavior of UNK.

The synthetic UNK occurs in two distinct compositional varieties: a Ti-rich variety (UNK) similar to that found in meteoritic samples that can be described in terms of the two components $Ca_3Al_2Si_4O_{14}$ and $Ca_3Ti_2^{3+}Al_2Si_2O_{14}$ and a Ti-poor, Si-rich variety (Si-UNK) on the same composition line, essentially $Ca_3Al_2Si_4O_{14}$. Like its meteoritic counterpart, synthetic UNK is characteristically high in TiO_2 and low in MgO (Table 2). Zoning in the largest crystals is similar to that found in meteoritic CAIs with cores higher in Ti and lower in Si than rims (Fig. 3b). Melilite surrounding larger UNK crystals is ~Ak_{50} (Figs. 5b, c), similar to that found surrounding UNK crystals in some Type B1 CAIs. In Fig. 2b, cations of Si are plotted *vs.* cations of Ti for synthetic UNK and Si-UNK analyses with Ca = 3.0 ± 0.05. The analyses all fall near the Si + Ti = 4.0 line on the graph. Those analyses plotting significantly above the line reflect contamination by intergrowths of melilite, glass, anorthite, pyroxene and a poorly characterized high Z phase. Compositions of meteoritic and synthetic UNKs are very similar with overlapping ranges in major oxides (Tables 1–2; Fig. 2). Only in Ti^{3+} contents are there significant differences (Fig. 4). The Si-UNKs crystallized in our experiments are compositionally distinct from both the Ti-rich meteoritic and synthetic UNK. This phase is characterized by 4 cations of Si in a formula unit based on a total of 9 cations and contains very little Mg or Ti (Table 2; Fig. 2b). It is possible that Si-UNK and UNK analyses shown in Fig. 4 lie on opposite limbs of a miscibility gap.

Textural Relationships–In an individual experimental charge, UNK occurs in one and only one of the four distinct petrographic associations illustrated in Fig. 7 and summarized by run conditions in Fig. 6. (1) UNK may occur as small (several μm) tabular crystals oriented along planes in melilite or filling the acute ends of glass pockets (Fig. 7a). This type of occurrence has been observed only in experiments on the 98 bulk composition with T_{max} = 1500 °C and CR = 2–20 °C/h. Meteoritic occurrences of UNK are texturally similar, although glass has not been observed. (2) Synthetic UNK from the 98 bulk composition can also form thin (5–10 μm) rims on melilite laths along with small prismatic crystals protruding from the ends of the melilite laths (Fig. 7b). (3) In CAI experiments, UNK is typically part of an intergrowth containing anorthite, melilite, pyroxene and UNK (Fig. 7c). One experiment on B2C also produced this texture. (4) UNK often crystallizes from the residual liquid between major phases in the sample (Fig. 7d). There is no obvious correlation between composition and textural type among the Ti-rich UNK.

The textural habit of Si-UNK is quite different from the Ti-bearing variety, appearing as a fibrous mass when viewed in

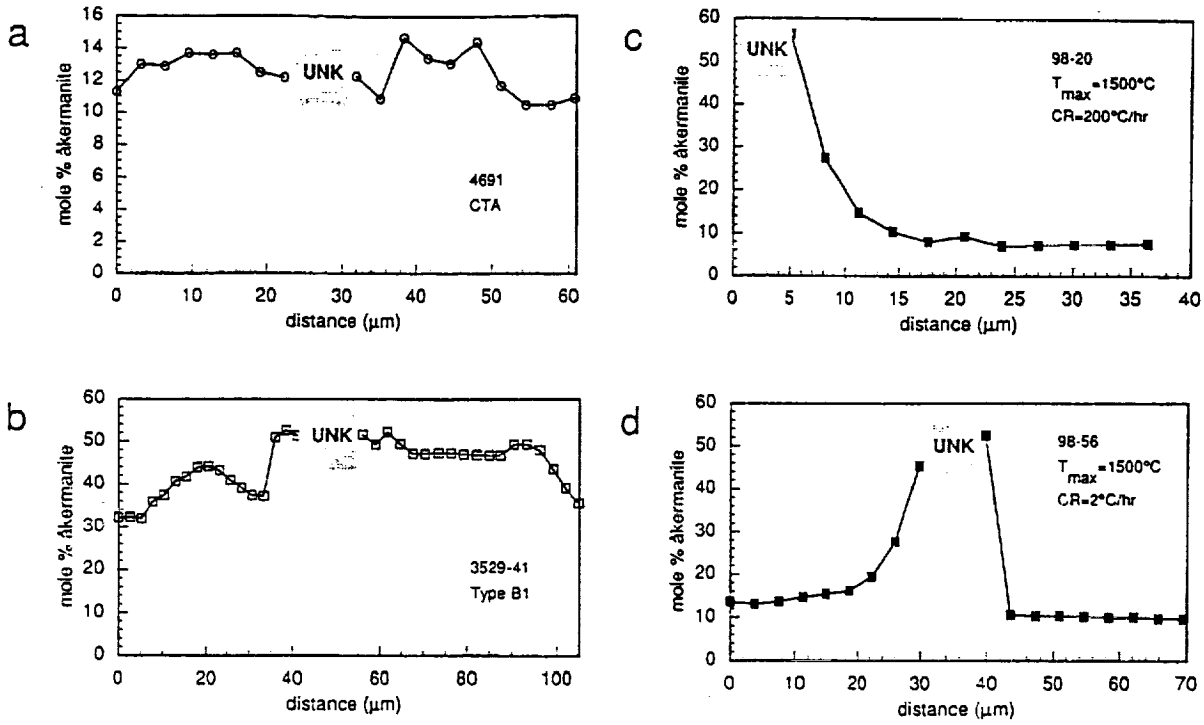

FIG. 5. Zoning in melilite surrounding, or adjacent to UNK. (a) Melilite surrounding UNK grain in NMNH 4691, a Compact Type A from Allende. (b) Melilite surrounding UNK grain in NMNH 3529-41, a Type B1 inclusions from Allende (see Fig. 1b). (c) Melilite adjacent to UNK formed as a rim on melilite laths (98-20; T_{max} = 1500 °C, CR = 200 °C/h). (d) Melilite composition surrounding UNK that crystallized from patches of liquid within the melilite (98-56; T_{max} =1500 °C, CR = 2 °C/h).

transmitted light. Figure 7e shows a backscattered electron image of one example. A very bright, hence, relatively high mean atomic number phase co-crystallizes with the Si-UNK. The phase contains significant concentrations of sulfur but has little, if any, Ti (*i.e.*, it might be oldhamite, but it is not perovskite or UNK). Due to the small grain size, the composition of this phase could not be quantified.

Factors Controlling the Crystallization of UNK in Experiments–Based on our results, UNK crystallizes from residual melts derived from a variety of CAI bulk compositions analogous to those of meteoritic inclusions, but the factors controlling the appearance of UNK are subtle because several sets of samples from the CAI bulk composition with identical T_{max}, cooling rate, and quench temperature, differ only in the presence or absence of UNK. This suggests that the statistical nature of nucleation plays a role (*e.g.*, Gibb, 1974) or that the appearance of UNK is controlled indirectly through changes in interstitial melt composition or boundary layer formation caused by crystallization of one or more of the phases melilite, spinel, anorthite and fassaite. Analyses of glass from multiple samples run under identical conditions are given in Table 3 and plotted in Fig. 8. Glass in samples containing UNK is significantly higher in MgO and lower in CaO than glass from samples run under identical conditions that did not produce UNK.

The phases spinel (sp), pyroxene, melilite (~Ak_{50}; mel) and anorthite (an) may also occur in UNK-bearing experimental run products and can potentially be used to constrain the thermodynamic properties of UNK. For example, if melilite, spinel and anorthite were simultaneously in equilibrium with UNK, then the activity of the Si-UNK component would be fixed *via* the reaction

$$4MgAl_2O_{4(sp)} + 7Ca_3Al_2Si_4O_{14(Si\text{-}UNK)} =$$

$$4Ca_2MgSi_2O_{7(Ak)} + 9CaAl_2Si_2O_{8(an)} + 2Ca_2Al_2SiO_{7(Ge)} . \quad \text{Equ. (1)}$$

However, some of the UNK-bearing glasses are not in equilibrium with spinel, based on the reaction

$$MgO_{(liq)} + Al_2O_{3(liq)} = MgAl_2O_{4(sp)}$$

and Berman's (1983) activity model for oxide components in the melt. This is probably due to overgrowths of pyroxene and/or melilite on the pre-existing spinel grains. In addition, nearly all of the glasses coexisting with UNK are supersaturated with respect to anorthite based on the reaction

$$CaO_{(liq)} + Al_2O_{3(liq)} + 2SiO_{2(liq)} = CaAl_2Si_2O_{8(an)}.$$

Equation (1) is, therefore, an inappropriate basis for interpreting our experiments. We can nevertheless crudely constrain the thermodynamic properties of the phase based on exchange equilibria involving components in the melt (liq). For the $Ca_3Al_2Si_4O_{14}$ component (*cf.* Fig. 4), the reaction

$$3CaO_{(liq)} + Al_2O_{3(liq)} + 4SiO_{2(liq)} = Ca_3Al_2Si_4O_{14(UNK)} \quad \text{Equ. (2)}$$

is applicable. An equilibrium constant for reaction (2) can be written

$$\ln K_{(2)} = \ln\left[\frac{a^{UNK}_{Si\text{-}UNK}}{(a^{liq}_{CaO})^3 (a^{liq}_{Al_2O_3})(a^{liq}_{SiO_2})^4}\right] = \frac{-\Delta G^{o}_{\rightarrow(2)}}{RT} , \quad \text{Equ. (3)}$$

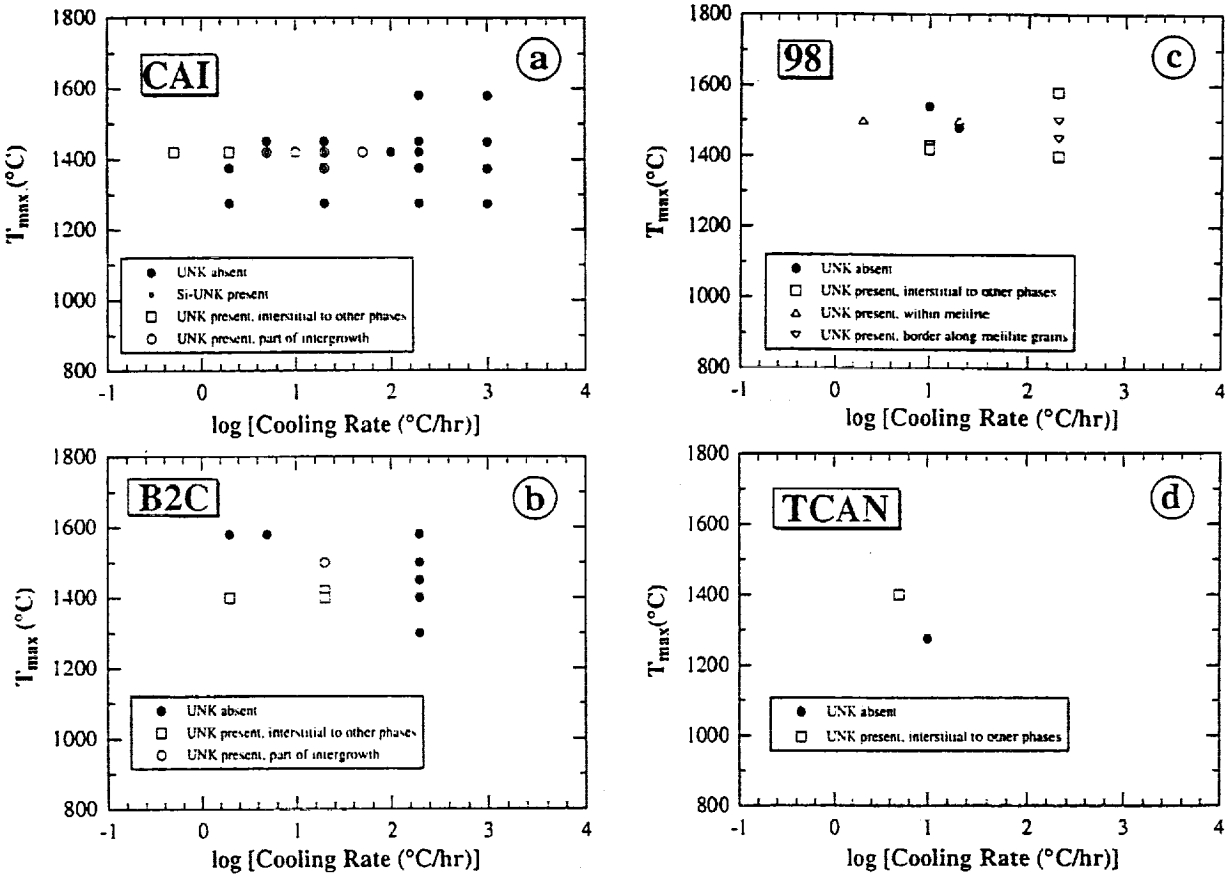

FIG. 6. Experimental conditions under which UNK is produced and the resulting textures. Each point represents a series of experiments in which samples were held at a maximum temperature for 3 h, cooled at a constant rate, and drop quenched at various temperatures. Open symbols indicate that one or more experiments in the series produced UNK. Only series including samples quenched from below 1100 °C are plotted. (a) CAI. (b) B2C. (c) 98. (d) TCAN.

or upon rearranging,

$$\ln K'_{(2)} = 3\ln(a^{liq}_{CaO}) + \ln(a^{liq}_{Al_2O_3}) + 4\ln(a^{liq}_{SiO_2}) = \frac{\Delta G^{o}_{(2)}}{RT} + \ln(a^{UNK}_{Si\text{-}UNK}) \cdot \quad \text{Equ. (4)}$$

TABLE 2. Selected analyses of UNK and Si-UNK from synthetic samples.

Sample	CAI-226	CAI-252	98-21	98-55	98-69	B2C-68	B2C-29	TCAN-32
Phase	UNK	Si-UNK	UNK	UNK	UNK	UNK	UNK	UNK
T_{max} (°C)	1420	1420	1500	1500	1500	1420	1400	1390
CR (°C/h)*	2	5	200	2	20	20	2	5
T_{quench} (°C)	1101	1001	1050	1071	1067	1025	1045	1042
Oxide wt%								
SiO_2	24.8	45.8	28.5	28.6	28.2	26.4	25.0	26.9
TiO_2	25.6	0.83	20.5	19.6	19.6	23.2	24.8	23.7
Al_2O_3	17.2	19.4	18.6	19.2	19.1	17.6	18.1	17.4
MgO	0.68	0.62	0.62	0.12	0.31	0.39	0.48	0.69
CaO	30.1	32.7	30.9	31.1	31.8	31.2	31.4	30.7
Total	98.4	99.4	99.1	98.6	99.0	98.8	99.8	99.4
Cations based on total = 9								
Si	2.29	3.92	2.57	2.60	2.54	2.41	2.35	2.44
Ti	1.77	0.05	1.40	1.34	1.33	1.59	1.57	1.62
Al	1.87	1.96	1.98	2.05	2.03	1.89	2.02	1.86
Mg	0.09	0.08	0.08	0.01	0.04	0.05	0.04	0.09
Ca	2.97	3.00	3.00	3.03	3.06	3.05	3.08	2.99
Si + Ti	4.06	3.97	3.97	3.94	3.87	4.00	3.92	4.06

* Cooling rate.

In Equations (3) and (4), a^i_j refers to the activity of component i in phase j, $\Delta G^{o}_{(2)}$ to the standard state free energy of reaction for equilibrium (2), R to the gas constant and T to the temperature in degrees K. The activity-composition relationships for UNK solid solutions are not known so activity and standard state terms on the right hand of Equ. (4) cannot be separated. $K'_{(2)}$ is that part of the equilibrium constant arising from activities of components in the melt. Given that the range in composition of the synthetic UNK is small (Fig. 4) and a $^{UNK}_{Si\text{-}UNK}$ may therefore be approximately constant, $K'_{(2)}$ may in fact be approximately constant for a given temperature. Using Berman's (1983) activity model for silicate melts (assuming that all Margules parameters involving TiO_2 are zero), $\ln K'_{(2)}$ was evaluated for synthetic glasses and plotted against inverse temperature for glass compositions from UNK-bearing and UNK-absent run products in Fig. 9a. A linear regression line,

$$\ln K'_{(2)} = 3\ln(a^{liq}_{CaO}) + \ln(a^{liq}_{Al_2O_3}) + 4\ln(a^{liq}_{SiO_2}) = -12.5 - \frac{1.84 \times 10^4}{T}$$

for the UNK-bearing experiments is also shown. We emphasize that this expression incorporates both standard state (free energy of formation from the solid oxides) and activity terms for the $Ca_3Al_2Si_4O_{14}$ component in UNK (*cf.* Equ. 4). This treatment also implicitly assumes that the composition of glass measured at some distance from crystals is the relevant measure of UNK stability

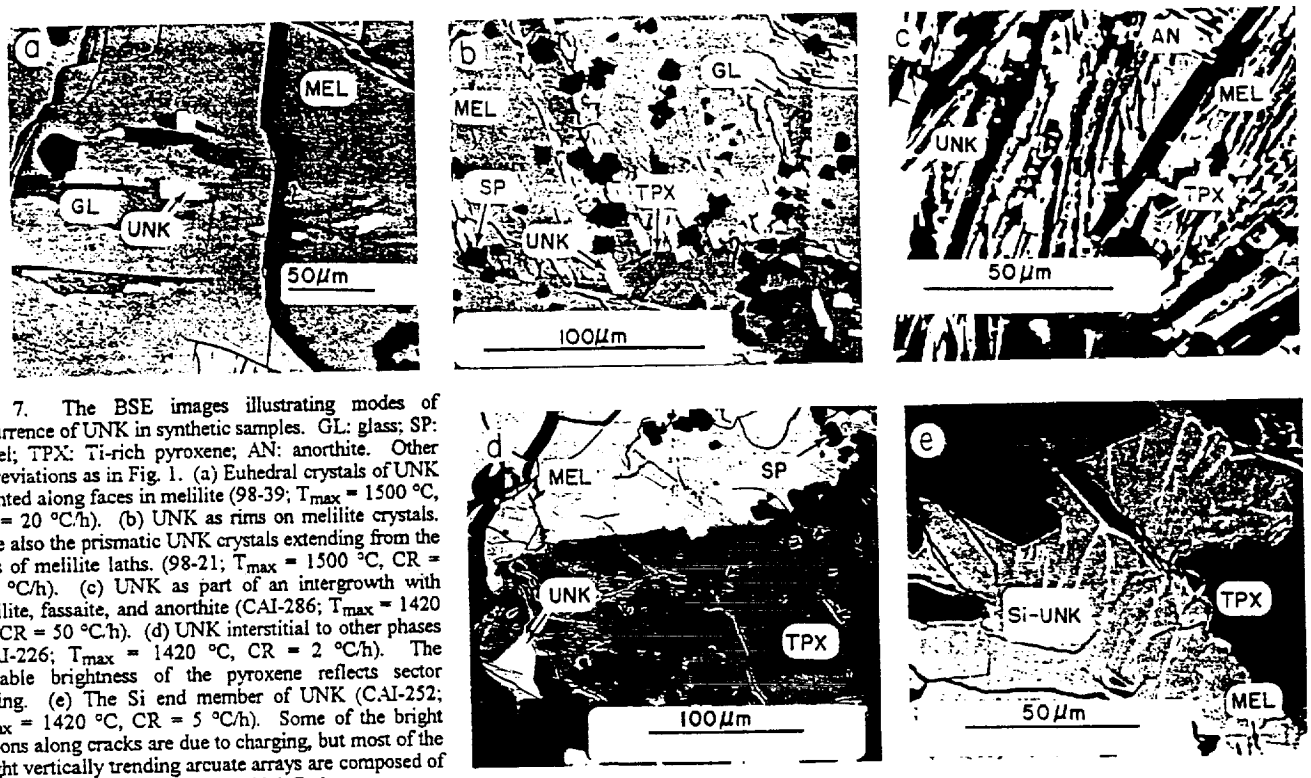

FIG. 7. The BSE images illustrating modes of occurrence of UNK in synthetic samples. GL: glass; SP: spinel; TPX: Ti-rich pyroxene; AN: anorthite. Other abbreviations as in Fig. 1. (a) Euhedral crystals of UNK oriented along faces in melilite (98-39; T_{max} = 1500 °C, CR = 20 °C/h). (b) UNK as rims on melilite crystals. Note also the prismatic UNK crystals extending from the ends of melilite laths. (98-21; T_{max} = 1500 °C, CR = 200 °C/h). (c) UNK as part of an intergrowth with melilite, fassaite, and anorthite (CAI-286; T_{max} = 1420 °C, CR = 50 °C/h). (d) UNK interstitial to other phases (CAI-226; T_{max} = 1420 °C, CR = 2 °C/h). The variable brightness of the pyroxene reflects sector zoning. (e) The Si end member of UNK (CAI-252; T_{max} = 1420 °C, CR = 5 °C/h). Some of the bright regions along cracks are due to charging, but most of the bright vertically trending arcuate arrays are composed of a poorly characterized, relatively high Z phase.

(*i.e.*, boundary layers are ignored). Nevertheless, liquid compositions from the UNK-bearing experiments are consistent with a single expression for $\ln K_{\dot{\omega}}$, which can be taken as approximating the conditions required for stabilizing UNK in CAI-like melts. The linearity suggests that either values of $a^{UNK}_{Si\text{-}UNK}$ for UNK in our experiments are all similar or that they change systematically with temperature. It is significant that glasses for all of the isothermal and most of the cooling rate experiments plot beneath the line in Fig. 9a (at lower values of 1/T) and, therefore, are predicted to be undersaturated with respect to UNK. This can explain simply why UNK is not observed in these experiments – it was never stable.

Figure 9b shows schematic curves of constant activity of the Si-UNK component for coexisting UNK and melt together with four schematic cooling paths in $\ln K_{\dot{\omega}} - 10^4/T$ for a CAI bulk composition. These curves can be used to illustrate factors influencing the appearance or non-appearance of UNK in a particular cooling sequence. The basis for our treatment is that as a particular bulk composition crystallizes, the residual melt moves to the right in the figure. If it reaches or crosses over the diagonal line in Fig. 9a defined by the UNK-saturated experiments, it becomes saturated or supersaturated with respect to UNK. Therefore, provided that nucleation can occur, we can expect to observe UNK in the run product. This treatment is necessarily schematic because precisely what a $^{UNK}_{Si\text{-}UNK}$ should be at saturation for a specific liquid is unknown (*i.e.*, we are unable to separate the contributions of $a^{UNK}_{Si\text{-}UNK}$ and $\Delta G^{\circ}_{(3)}$ to $\ln K_{\dot{\omega}}$) and because we are neglecting the activities of other components in the melt and UNK. In particular, the Ti-content of the UNK and melt are important in determining saturation. For example, UNK saturation may not be possible in a specific instance because the Ti-content of the melt may be insufficient to stabilize Ti-bearing UNK with the appro-priate $a^{UNK}_{Si\text{-}UNK}$. The present analysis, therefore, should be viewed as providing necessary but insufficient conditions for the stability of UNK. Keeping these caveats in mind, CAI-like melts with $\ln K_{\dot{\omega}}$ plotting beneath a particular isoactivity line will to first order be undersaturated with respect to UNK of a given activity, and hence of some composition, provided that $a^{UNK}_{Si\text{-}UNK}$ is physically achievable. Melts with $\ln K_{\dot{\omega}}$ plotting above an isoactivity line will be supersaturated with respect to that UNK. Any melt with $\ln K_{\dot{\omega}}$ plotting above the $a^{UNK}_{Si\text{-}UNK} = 1$ line will be supersaturated with respect to Si-rich UNK regardless of the UNK composition.

For illustrative purposes, we consider a "zone", represented by the UNK-saturated points in Fig. 9a and by the roughly parallel lines of constant $a^{UNK}_{Si\text{-}UNK}$ in Fig. 9b, where saturation with respect to UNK is possible. Upon cooling of a droplet of CAI bulk composition from above the liquidus, first spinel and then melilite + spinel crystallize with decreasing temperature. The melt changes composition, but $\ln K_{\dot{\omega}}$ increases only slightly based on liquid lines of descent determined experimentally. In path A, UNK saturation is reached before any other additional phases crystallize. UNK crystallizes, and $\ln K_{\dot{\omega}}$ changes along an UNK-saturated path. In detail, $a^{UNK}_{Si\text{-}UNK}$ changes as the composition of UNK and other phases change, but the precise path is not quantified by our experiments. In path B, pyroxene crystallizes before UNK, and $\ln K_{\dot{\omega}}$ decreases relative to a pyroxene-absent liquid line of descent. This has the effect of delaying the appearance of UNK of a given

TABLE 3. Comparison of glass analyses from CAI bulk composition samples with and without UNK, all other conditions equal.

Run #	263*	264*	265*	288	287*	290	289*
T_{max} (°C)	1420	1420	1420	1420	1420	1420	1420
CR (°C/h)†	2	2	2	50	50	50	50
T_{quench} (°C)	1048	1048	1048	1117	1117	1059	1059
UNK?**	yes	no	no	yes	no	yes	no
			Oxide wt%				
SiO_2	42.7	44.8	44.9	42.3	43.3	42.3	45.9
TiO_2	1.37	0.58	0.55	3.53	1.53	3.23	1.75
Al_2O_3	18.2	20.3	21.9	20.9	19.2	21.9	14.0
MgO	10.8	1.05	0.71	5.8	2.93	4.79	1.30
CaO	27.0	31.3	29.7	25.7	30.7	24.5	34.3
Total	100.1	98.0	97.8	98.2	97.7	96.7	97.3

* Average of two analyses.

† Cooling rate.

** All samples containing UNK have the phase assemblage glass – spinel + melilite + Ti fassaite + anorthite + UNK. Samples without UNK have the phase assemblage glass + spinel + melilite + Ti-fassaite. CAI-289 also contains anorthite.

a_{Si-UNK}^{UNK} to lower temperatures. If pyroxene begins to crystallize early enough, UNK saturation may be delayed to such low temperatures that UNK never crystallizes (path C). It is possible that anorthite has an effect similar to that of pyroxene, although our data are insufficient to confirm this. In path D, no additional phases join melilite and spinel and eventually the melt becomes supersaturated with respect to UNK (as well as for other phases such as anorthite and pyroxene).

The four paths illustrated schematically in Fig. 9b can also help to rationalize the association of UNK with particular ranges in experimental conditions (Fig. 6) because they are crudely correlated with T_{max} and cooling rate. For CAI experiments cooled at intermediate to rapid cooling rates from T_{max} ~ 1420 °C, near melilite saturation for the CAI bulk composition (Stolper, 1982), the liquid line of descent intersects the temperature-liquid composition regime within which UNK can crystallize because the appearances of anorthite and fassaite are delayed so that UNK is stabilized at relatively high temperatures (*e.g.*, path A in Fig. 9b) and, therefore, can crystallize provided appropriate nucleation sites are available. UNK crystallization for T_{max} ~ 1420 °C is unlikely at the highest cooling rates because, although the liquid compositions pass through an appropriate region of $\ln K_{\dot{\omega}} - 1/T$ for UNK crystallization, there is insufficient time for nucleation of UNK (or indeed of pyroxene or anorthite in many cases). At higher T_{max}, crystallization of all of the silicates including UNK are greatly suppressed relative to their equilibrium appearance temperatures (Stolper and Paque, 1986) due to destruction of nuclei. Therefore, the probability that UNK will crystallize is

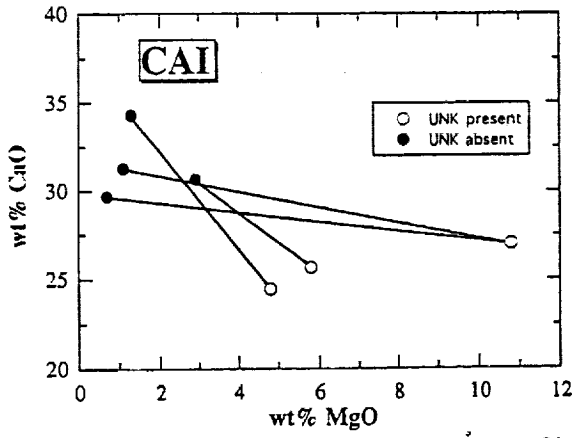

FIG. 8. Wt% CaO *vs.* wt% MgO in glass from CAI experiments. Lines join samples with and without UNK that were run under identical conditions at the same time.

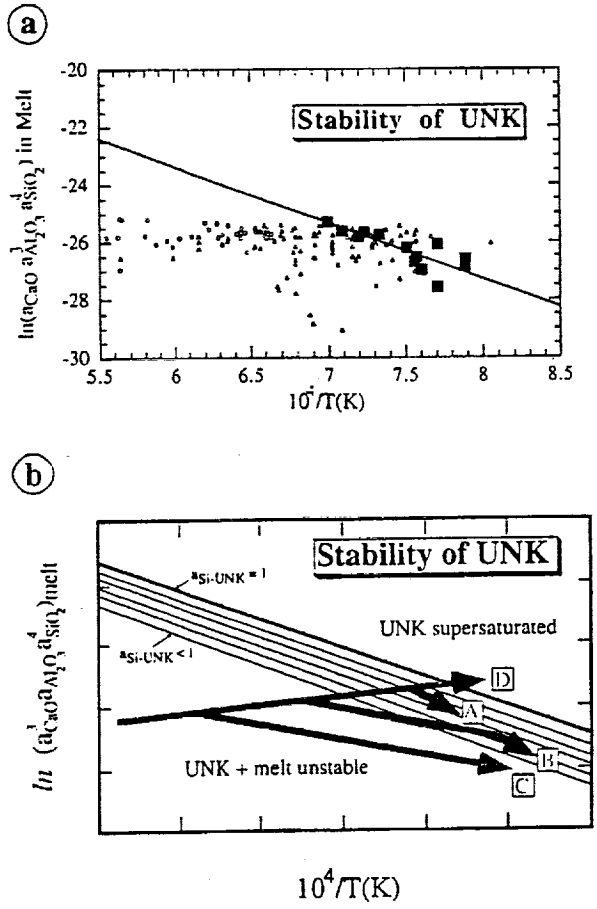

FIG. 9. Stability of UNK. (a) Experimental results. Oxide activities in the melt were obtained using Berman's (1983) model and are relative to solid lime, corundum and cristobalite. Closed squares represent UNK-bearing controlled cooling rate experiments in which the phases spinel, melilite, pyroxene, anorthite, UNK and glass are all present. Isothermal experiments (open circles) and cooling rate experiments (open triangles) for which UNK was not observed, represent various phase assemblages. (b) Four schematic liquid lines of descent for an initially molten liquid of bulk CAI composition in terms of $\ln K_{\infty} - 10^4/T$. Curve A: spinel → spinel + melilite → spinel + melilite + UNK (pyroxene fails to nucleate before UNK; intermediate to high T_{max}, low to intermediate cooling rates). Curve B: spinel → spinel + melilite → spinel + melilite + pyroxene → spinel + melilite + pyroxene + UNK (pyroxene crystallizes before UNK and delays but does not prevent later UNK crystallization; intermediate T_{max} and cooling rate). Curve C: spinel → spinel + melilite → spinel + melilite + pyroxene (pyroxene appears at a high enough temperature to completely suppress UNK crystallization; low T_{max} and cooling rate). Curve D: spinel → spinel + melilite (pyroxene and UNK fail to nucleate; high T_{max} and cooling rate). Thermal histories in which one or both of melilite and spinel failed to nucleate (*i.e.*, high T_{max} with very fast cooling rates) would lead to paths similar to D though with somewhat different slopes.

reduced at all cooling rates (path D in Fig. 9b). At lower T_{max} and cooling rates, pyroxene begins to crystallize at a higher temperature (paths B and C in Fig. 9b) so that the appearance of UNK is suppressed as discussed above. UNK may still crystallize (curve B) if cooling rates are not so slow that the early appearance of pyroxene leads to entirely suppressing UNK stability under igneous conditions (curve C). The probability of encountering UNK therefore decreases for both higher and lower T_{max} and for very high cooling rates. The data base is less complete for the B2C and 98 bulk compositions but the results are consistent with the same basic behavior.

Origin of UNK

There are several possible modes of origin for UNK in meteorites, including crystallization from a late-stage residual liquid, exsolution from the enclosing melilite, or alteration. It should be emphasized that different occurrences of meteoritic UNK may have different modes of origin. Here, we address the possibility that meteoritic UNK crystallized from a melt. A general discussion of other possibilities is given in Barber *et al.*(1994)

Based on Fig. 9a, UNK will not be stabilized as a near-liquidus phase for any of the Types A, B, or C inclusions described by Wark (1981), Wark and Lovering (1982), Beckett (1986), or Wark (1987) because ln $K_{(i)}$ is too low. The dynamic crystallization experiments demonstrate that UNK with composition very similar to meteoritic examples can crystallize from a range of bulk compositions representing these CAIs but only from very late stage liquids after extensive crystallization of melilite and spinel ± anorthite ± fassaite, which drive the residual liquid near to UNK saturation. If meteoritic UNK crystallized from a melt, it, therefore, must have formed late in the crystallization sequence, but this poses potential problems for meteoritic occurrences of UNK described in this work. UNK is included in texturally early melilite at least in Type B1 inclusions (*i.e.* it is preferentially in the outer portions of the melilite mantle), although it is possible that meteoritic UNK in the melilite mantle is actually a late-crystallizing phase analogous to fassaite inclusions in mantle melilites (MacPherson *et al.*, 1984; Simon *et al.*, 1991) and the increase in X_{Ak} near UNK inclusions (Fig. 5b) is consistent with this. If meteoritic UNK formed by such a mechanism, then extreme rare earth element (REE) enrichments would be expected whereas its REE content would be expected to be low if it had exsolved from the surrounding melilite. The UNK described by El Goresy *et al.* (1984) is REE enriched and, therefore, consistent with crystallization from a melt, but the host inclusion is so unusual that it is not possible based on this occurrence to make general inferences about occurrences of UNK in the Allende CAIs described here. There are currently no REE analyses of UNK from these CAIs. Another problem with crystallization of meteoritic UNK from a melt is that glass is often associated with UNK included in melilite in experimental samples, but this feature is not observed in CAIs. Floss *et al.* (1992) described a phase similar to UNK occurring as symplectic intergrowths in a Compact Type A inclusion apparently replacing perovskite. The phase is enriched in REE and although subsolidus reactions may be responsible, crystallization from near-solidus melts is a more likely origin for this type of texture.

Regardless of its origin the invariably low Mg and relatively high Al contents of UNK make it potentially useful for ^{26}Al studies analogous to those on corundum and anorthite (Podosek *et al.*, 1991; Virag *et al.*, 1991). The grains may yield useful information on the timing of whatever event produced them. Finally, it is worth noting that if a significant proportion of the Ti in meteoritic UNK coexisting with perovskite is trivalent (*e.g.*, Floss *et al.*, 1992), then quantitative calibration of oxygen barometers such as

$$3Ca_3Ti^{4+}Al_2Si_3O_{14} - 3CaTiO_3 = 3Ca_2Al_2SiO_7 + 2Ca_3Ti^{4+}Ti^{3+}_2Si_3O_{14} + O_2$$

could provide useful insight into redox conditions.

CONCLUSIONS

UNK is found as small, tabular inclusions in melilite in approximately half of the Type A and B1 CAIs examined. It contains small amounts of Ti^{3+} (7–13% of total Ti) suggesting growth under reducing conditions. UNK of similar composition is produced in dynamic crystallization experiments over a well-defined range of maximum temperatures and cooling rates. The crystallization of UNK from CAI-like bulk compositions requires residual melt compositions unlike those found under equilibrium conditions, thereby explaining its restriction to dynamic crystallization experiments, which generate a wider range of liquid compositions, some of which reach saturation with respect to UNK.

Acknowledgments–Reviews of A. El Goresy and G. J. MacPherson led to substantive improvements in the manuscript. This work was supported by NASA grants NAG 9-105 and NAGW- 3533 to EMS, NAG 9-28 to John Wood, and SETI grant NCC 2-758 to Laurance Doyle. Caltech Division of Geological and Planetary Sciences, Division Contribution No. 5215.

Editorial handling: K. Keil

REFERENCES

AGRELL S. O. (1945) Mineralogical observations on some basic open-hearth slags. *J. Iron Steel Inst. Lond.* **152**, 19P–55P.

ALBEE A. L. AND RAY L. (1970) Correction factors for electron probe microanalysis of silicates, oxides, carbonates, phosphates, and sulfates. *Anal. Chem.* **42**, 1408–1414.

BARBER D. J. AND AGRELL S. O. (1994) A new titanium-bearing calcium aluminosilicate phase: III. Crystals from a mixer furnace slag. *Meteoritics* **29**, 691–695.

BARBER D. J., BECKETT J. R., PAQUE J. M. AND STOLPER E. (1994) A new titanium-bearing calcium aluminosilicate phase: II. Crystallography and crystal chemistry of grains formed in slowly cooled melts with bulk compositions of calcium-, aluminum-rich inclusions. *Meteoritics* **29**, 682–690.

BECKETT J. R. (1986) The origin of calcium-, aluminum-rich inclusions from carbonaceous chondrites: An experimental study. Ph.D. thesis, University of Chicago. 373 pp.

BECKETT J. R. AND STOLPER E. (1994) The stability of hibonite, melilite and other aluminous phases in silicate melts: Implications for the origin of hibonite-bearing inclusions from carbonaceous chondrites. *Meteoritics* **29**, 41–65.

BECKETT J. R., SPIVACK A. J., HUTCHEON I. D., WASSERBURG G. J. AND STOLPER E. M. (1990) Crystal chemical effects on the partitioning of trace elements between mineral and melt: An experimental study of melilite with applications to refractory inclusions from carbonaceous chondrites. *Geochim. Cosmochim. Acta* **54**, 1755–1774.

BERMAN R. G. (1983) A thermodynamic model for multicomponent melts with application to the system CaO-MgO-Al_2O_3-SiO_2. Ph.D. thesis, University of British Columbia. 178 pp.

DEER W. A., HOWIE R. A. AND ZUSSMAN J. (1992) *An Introduction to the Rock-forming Minerals.* Longman Scientific and Technical Press, Essex, U. K. 696 pp.

EL GORESY A., PALME H., YABUKI H., NAGEL K., HERRWERTH I. AND RAMDOHR P. (1984) A calcium-aluminum-rich inclusion from the Essebi (CM2) chondrite: Evidence for captured spinel-hibonite spherules and for

an ultra-refractory rimming sequence. *Geochim. Cosmochim. Acta* 48, 2283–2298.

FLOSS C., EL GORESY A., PALME H., SPETTEL B. AND ZINNER E. (1992) An unusual Ca-Ti-Al silicate in a Type A Allende inclusion (abstract). *Meteoritics* 27, 220.

GIBB F. G. F. (1974) Supercooling and the crystallization of plagioclase from a basaltic magma. *Mineral. Mag.* 39, 641–653.

MACPHERSON G. J., PAQUE J. M., STOLPER E. AND GROSSMAN L. (1984) The origin and significance of reverse zoning in melilite from Allende Type B inclusions. *J. Geol.* 92, 289–305.

MACPHERSON G. J., WARK D. A. AND ARMSTRONG J. T. (1988) Primitive material surviving in chondrites: Refractory inclusions. In *Meteorites and the Early Solar System* (eds. J. F. Kerridge and M. S. Matthews), pp. 746–807. Univ. Arizona Press, Tucson, Arizona.

PAQUE J. M. AND STOLPER E. (1984) Crystallization experiments on a range of Ca-Al-rich inclusion compositions (abstract). *Lunar Planet. Sci.* 15, 631–632.

PAQUE J. M., BECKETT J. R. AND STOLPER E. (1986) A new Ca-Al-Ti silicate in coarse-grained Ca-Al-rich inclusions (abstract). *Lunar Planet. Sci.* 17, 646–647.

PODOSEK F. A., ZINNER E. K., MACPHERSON G. J., LUNDBERG L. L., BRANNON J. C. AND FAHEY A. J. (1991) Correlated study of initial $^{87}Sr/^{86}Sr$ and Al-Mg isotopic systematics and petrologic properties in a suite of refractory inclusions from the Allende meteorite. *Geochim. Cosmochim. Acta* 55, 1083–1110.

SIMON S. B., GROSSMAN L. AND DAVIS A. M. (1991) Fassaite composition trends during crystallization of Allende Type B refractory inclusion melts. *Geochim. Cosmochim. Acta* 55, 2635–2655.

STOLPER E. (1982) Crystallization sequences of Ca-Al-rich inclusions from Allende: An experimental study. *Geochim. Cosmochim. Acta* 46, 2159–2180.

STOLPER E. AND PAQUE J. M. (1986) Crystallization sequences of Ca-Al-rich inclusions from Allende: The effects of cooling rate and maximum temperature. *Geochim. Cosmochim. Acta* 50, 1785–1806.

VIRAG A., ZINNER E., AMARI S. AND ANDERS E. (1991) An ion microprobe study of corundum in the Murchison meteorite: Implications for ^{26}Al and ^{16}O in the early solar system. *Geochim. Cosmochim. Acta* 55, 2045–2062.

WARK D. A. (1981) The pre-alteration compositions of Allende Ca-Al-rich condensates (abstract). *Lunar Planet. Sci.* 12, 1148–1150.

WARK D. A. (1987) Plagioclase-rich inclusions in carbonaceous chondrite meteorites: Liquid condensates? *Geochim. Cosmochim. Acta* 51, 221–242.

WARK D. A. AND LOVERING J. F. (1982) The nature and origin of type B1 and B2 Ca-Al-rich inclusions in the Allende meteorite *Geochim. Cosmochim. Acta* 46, 2581–2594.

A new titanium-bearing calcium aluminosilicate phase: II. Crystallography and crystal chemistry of grains formed in slowly cooled melts with bulk compositions of calcium- aluminum-rich inclusions

DAVID J. BARBER[1]*, JOHN R. BECKETT[2], JULIE M. PAQUE[3] AND EDWARD STOLPER[2]

[1]Physics Department, University of Essex, Colchester, Essex CO4 3SQ, U. K.

[2]Division of Geological and Planetary Sciences, California Institute of Technology, Pasadena, California 91125 USA

[3]SETI Institute, NASA-Ames Research Center, MS 244-11, Moffett Field, California 94305 USA

*Current address: Physics Department, The Hong Kong University of Science and Technology, Clear Water Bay, Kowloon, Hong Kong

(Received 1993 September 28; accepted in revised form 1994 May 3)

Abstract—The crystallography and crystal chemistry of a new calcium-titanium-aluminosilicate mineral (UNK) observed in synthetic analogs to calcium-aluminum-rich inclusions (CAIs) from carbonaceous chondrites was studied by electron diffraction techniques. The unit cell is primitive hexagonal or trigonal, with $a = 0.790 \pm 0.002$ nm and $c = 0.492 \pm 0.002$ nm, similar to the lattice parameters of melilite and consistent with cell dimensions for crystals in a mixer furnace slag described by Barber and Agrell (1994). The phase frequently displays an epitactic relationship in which melilite acts as the host, with $(0001)_{UNK} \parallel (001)_{mel}$ and $\langle 10\bar{1}0\rangle_{UNK} \parallel \langle 100\rangle_{mel}$. If one of the two space groups determined by Barber and Agrell (1994) for their sample of UNK is applicable (P3ml or P31m), then the structure is probably characterized by puckered sheets of octahedra and tetrahedra perpendicular to the c-axis with successive sheets coordinated by planar arrays of Ca. In this likely structure, each unit cell contains three Ca sites located in mirror planes, one octahedrally coordinated cation located along a three-fold axis and five tetrahedrally coordinated cations, three in mirrors and two along triads. The octahedron contains Ti but, because there are 1.3–1.9 cations of Ti/formula unit, some of the Ti must also be in tetrahedral coordination, an unusual but not unprecedented situation for a silicate. Tetrahedral sites in mirror planes would contain mostly Si, with lesser amounts of Al while those along the triads correspondingly contain mostly Al with subordinate Ti. The structural formula, therefore, can be expressed as

$$Ca_3^{VIII}(Ti,Al)^{VI}(Al,Ti,Si)_2^{IV}(Si,Al)_3^{IV}O_{14}$$

with Si + Ti = 4. Compositions of meteoritic and synthetic Ti-bearing samples of the phase can be described in terms of a binary solid solution between the end-members $Ca_3TiAl_2Si_3O_{14}$ and $Ca_3Ti(AlTi)(AlSi_2)O_{14}$. A Ti-free analog with a formula of $Ca_3Al_2Si_4O_{14}$ synthesized by Paque *et al.* (1994) is thought to be related structurally but with the octahedral site being occupied by Al, that is,

$$Ca_3^{VIII}Al^{VI}(Al,Si)_2^{IV}(Si)_3^{IV}O_{14}\ .$$

INTRODUCTION

Coarse-grained calcium-aluminum-rich inclusions (CAIs) in carbonaceous chondrites have chemical and isotopic signatures indicative of processes dating back to the origin and earliest evolution of the Solar System (see Grossman, 1980 and MacPherson *et al.*, 1988 for reviews). The mineralogy is generally dominated by a combination of one or more of clinopyroxene, melilite, spinel, anorthite, hibonite and perovskite. For each phase, the compositions and textures reflect the history of the host inclusion and can be used to impose constraints on physical conditions early in the Solar System. There are, in addition, various minor and trace minerals in CAIs including a new Ca-Ti-Al silicate described by El Goresy *et al.* (1984) and Paque *et al.* (1986). This phase could also contain genetic information about CAIs, but the crystal structure, phase relations, thermodynamic and kinetic properties that might allow such information to be extracted have not been characterized. In this study, we consider the crystal structure of the phase. The mineral remains unnamed because there are no x-ray diffraction (XRD) data currently available on the natural material, but for the purposes of this paper, we refer to the phase as UNK.

UNK is a ubiquitous, albeit minor, constituent of coarse-grained melilite-rich (Type A: Grossman, 1975) and fassaite-rich (Type B) CAIs. In occurrences of UNK reported thus far (El

Goresy *et al.*, 1984; Paque *et al.*, 1986, 1994), only small (<40 μm diameter) grains enclosed in melilite have been observed. Larger (~100 μm) grains of a phase similar to UNK in a Type A inclusion from Allende were described by Floss *et al.* (1992), but these crystals have higher Ca contents than UNK and different cell dimensions (A. El Goresy, pers. comm., 1992). Optically, UNK can be distinguished from fassaite, which has similar relief and reflectivity, by a lack of pleochroism, the presence of parallel extinction and, in the largest crystals, by its third order interference colors, which are consistent with indices of refraction determined by Barber and Agrell (1994) on synthetic crystals from a mixer furnace slag. UNK is also chemically distinctive. The formula, based on 14 oxygens, can be represented by $Ca_3Ti(Al,Ti)_2(Si,Al)_3O_{14}$, although neither the two sites occupied by Al + Ti nor the three sites occupied by Al + Si are necessarily crystallographically equivalent. With TiO_2 contents greater than 20 wt%, UNK is more titanian than all but the most Ti-rich of fassaites in CAIs, while MgO contents are quite low (<1 wt%), contrasting with the 5–10 wt% MgO typical of the fassaite. Rhönite, another Ca-Al-Ti-rich phase occasionally encountered in CAIs (Fuchs, 1978) is strongly pleochroic and distinguishable chemically from UNK by its much higher MgO (~17 wt% *vs.* <1) and lower CaO (~18 wt% *vs.* ~31) contents.

Synthetic crystals with compositions and optical properties very similar to those of meteoritic UNK were produced as a late-crystallizing phase in cooling rate experiments on a variety of CAI-like bulk compositions (Paque and Stolper, 1984; Stolper and Paque, 1986; Beckett and Stolper, 1994; Paque *et al.*, 1994). In these experiments, a powdered glassy starting material was held at a maximum temperature, usually for 3 h, cooled at a constant rate and then quenched into deionized H_2O. UNK was produced over a wide range of maximum temperatures and cooling rates for these bulk compositions (Paque *et al.*, 1994). Its occurrence in these experiments was controlled by the generation of residual melt compositions that intersect the UNK stability field and possibly by nucleation probabilities (Paque *et al.*, 1994). Attempts to crystallize UNK from melts with bulk compositions approximating those of UNK failed due to the crystallization of large amounts of perovskite (*i.e.*, UNK is unstable in a melt of its own composition).

This is the second of three papers describing the crystal chemistry and petrogenesis of UNK. In the first paper (Paque *et al.*, 1994), the characteristics of meteoritic and synthetic UNK and the conditions under which they can be produced are described. In this paper, we report the results of chemical and structural characterization of UNK from the run product of a cooling rate experiment on bulk composition 98 (Paque and Stolper, 1984), an analog for Allende inclusion USNM 3898 and typical of compact Type A CAIs or unusually melilite-rich Type B1s. The small grain sizes and great difficulty of obtaining reasonably pure separates of UNK precluded a structure determination by routine XRD methods. We, therefore, explored the crystal structure by using conventional electron diffraction and convergent beam electron diffraction (CBED) in conjunction with analytical transmission electron microscopy (ATEM). In the third paper of this series (Barber and Agrell, 1994), an occurrence of UNK from a furnace slag is described. Using CBED methods (Steeds, 1979; Williams, 1984; Champness, 1987), we establish that the space group of crystals from the slag is either P3m1 or P31m; therefore, we use four-digit Miller-Bravais indices and hexagonal axes throughout this paper in describing the crystallography of UNK.

EXPERIMENTAL PROCEDURES

Synthesis

Experimental procedures were similar to those described by Stolper and Paque (1986). Starting materials were synthesized by weighing out appropriate amounts of $CaCO_3$ and the oxides MgO, SiO_2, TiO_2 and Al_2O_3 (all ALFA Puratronic) for the bulk composition of interest, followed by grinding in an automatic agate mortar under ethanol for 5 h, decarbonation at ~1000 °C for 2 days and melting in a Pt crucible for 30 h in air at 1585 °C. Experiments were conducted in air in a home-built $MoSi_2$ vertical tube furnace. Temperatures were measured using a bare Pt/Pt-10Rh thermocouple and were controlled by a Eurotherm Model 818 programmer. To produce sufficient quantities of UNK for characterization by transmission electron microscopy (TEM), a large volume (1 g; sample designated 86C-4) of the 98 bulk composition was held in a Pt crucible at 1500 °C for 3 h, cooled at 20 °C/h to 946 °C and quenched through the top of the furnace into deionized H_2O. Previous work (Paque *et al.*, 1994) had shown that UNK would crystallize from the 98 bulk composition if subjected to such a thermal history, and indeed, the run product consisted mostly of melilite, lesser amounts of fassaite and spinel, and trace UNK.

Electron Microprobe Analysis and Scanning Electron Microscopy

Wavelength dispersive analyses were carried out on an electron microprobe designed and constructed in the Department of Earth Sciences at the University of Cambridge with an Si(Li) detector and a 40° take-off angle linked to a Harwell Highspec 3073 pulse processor and interfaced to a Nova 2 minicomputer. It was operated at 20kV and gives a relative precision of ~2% for major elements (*i.e.*, those elements at >5 wt%).

Transmission Electron Microscopy

The run product from 86C-4 was coarsely crushed, chunks were mounted in epoxy resin, ground flat and then polished. The polished surfaces were examined by reflected light microscopy, and the positions of UNK crystals as judged by relief and contrast were noted and photographed. Each mount was then coated with Pd-Au and examined in an SEM equipped with an energy dispersive analyzer in order to confirm the identity of UNK in the polished face, hereafter called face A. A typical example is shown in Fig. 1. Mounts that contained the UNK phase were then cemented, face A downwards, onto glass slides by means of "Crystalbond" resin and reduced in thickness to about 40 μm by grinding and polishing. The resulting thin sections were demounted, and all traces of the resin removed with acetone. Finally, aperture-type Cu electron microscope grids, with hole diameters of either 0.4 or 0.6 mm, were resin-bonded to the A-faces of pieces of the thin sections, thereby positioning an UNK crystal centrally within each aperture.

Ion-beam-milling from opposite the A-face was used to erode the specimen surface until the material was very thin in the proximity of the UNK phase. Both ion beam sources were then used for final milling to electron transparency. This process was not straightforward because UNK is usually surrounded by melilite, which sputters away faster than any other phase in the sample and also tends to crack during ion milling. As a result, UNK crystals were often lost

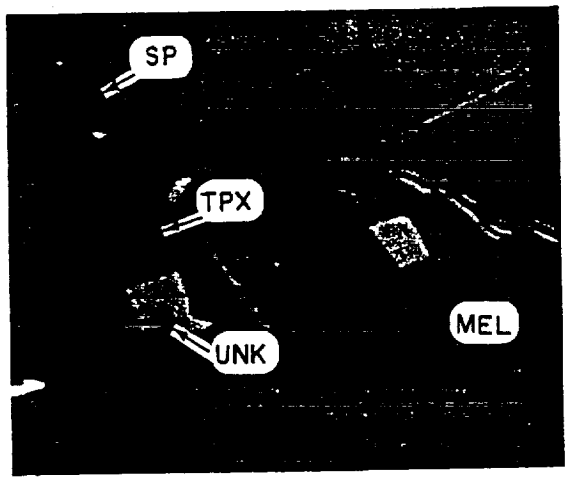

FIG. 1. Back-scattered electron SEM image of prismatic UNK grain together with spinel (SP) and Ti-fassaite (TPX) in melilite (MEL). Scale bar is 100 μm.

from the mounts before they were thin enough for investigation by ATEM. Surviving specimens were coated with a thin layer of C prior to insertion in the electron microscope, in order to prevent electrical charging.

The ATEM work was carried out on two instruments: a JEOL 200-CX instrument fitted with free-lens controls and scanning-type objective pole pieces, and a Philips CM12 microscope. Both microscopes were equipped with Be-window energy dispersive X-ray analysis (EDX) systems and spectrum-processing routines based on the Cliff and Lorimer (1975) ratio method for determining element concentrations. Cliff-Lorimer k-factors were available for each microscope, determined experimentally from material standards. For electron diffraction, the 200-CX was operated at 200 kV and the CM12 at 120 kV. For microanalysis by EDX, the 200-CX was operated at 120 kV using the "free lens" controls to form small electron probes. Specimens were examined in both the 200-CX and the CM12 modes by means of eucentric double-tilting goniometer holders, giving maximum rotations of ±45°, ±60°, and ±15°, ±45° respectively, where the first figure in each pair corresponds to the tilt axis and the second to rotation about the axis of the "pencil"-type holder. All accurate orientating of UNK crystals to characterize the reciprocal cell was carried out with the 200-CX. The "pencil" (roll) axis of this instrument has a vernier scale and is, in principle, capable of giving angles accurate to ±0.2°. Both goniometer scales were calibrated by recording the angular readings when the electron beam was successively set parallel to the <100> and <110> zone axes of single crystal MgO. Settings of the tilt axis (*i.e.*, the axis orthogonal to the "pencil" axis) were found to be irreproducible and, therefore, unreliable because of slippage in the tilt-drive mechanism: this limited the ways in which the crystallographic investigations could be carried out.

For maximum precision in microanalysis, grid-mounted specimens were placed in a graphite insert of the single-axis-tilt sample holder of the 200-CX. At a late stage in the study, selected area electron diffraction (SAD) patterns from UNK were accurately calibrated by evaporating a thin (~30 nm) film of Au onto selected specimens to give superposed ring patterns from the metal. Measurements of distances in zone axis SADs were made directly from the negatives with the aid of a Joyce Loebl recording microdensitometer.

As explained later, we attempted to determine the full symmetry of the UNK crystals by means of the CBED method. Experiments were first carried out by operating the 200-CX instrument in the "free lens control mode" with the objective lens overfocussed (Goodman, 1980), but later work mostly involved the CM12. In practice, the CAI-melt-derived crystals gave CBED patterns that lacked detail, even after specimens were further lightly sputter-thinned at low accelerating voltages and at glancing angles to reduce the thickness of radiation-damaged surface layers. A double-tilt goniometer stage cooled by liquid-nitrogen was also used in an attempt to obtain better convergent beam diffraction, but this too failed to yield any significant improvements.

RESULTS

General Observations by ATEM

The synthetic crystals of UNK have no unusual or distinctive microstructural characteristics when viewed by TEM, in contrast to most phases in CAIs (Barber *et al.*, 1984). This most likely reflects the simple thermal histories of the synthetic material. Dislocation densities are extremely low except at the crystal peripheries where the phase is sometimes intergrown with other minerals. Nor is there any evidence for ordered domains in TEM images or for superstructure reflections in the diffraction patterns. Microanalyses by ATEM show a modest spread in composition in general agreement with the results of Paque *et al.* (1986; 1994). The slight core-to-rim chemical zonation reported by Paque *et al.* was also apparent in some crystals, but no other chemical heterogeneities were found.

The most interesting morphological finding is the existence of an epitactic relationship between UNK and adjacent melilite. Several instances of this epitaxial contact were observed. Figure 2 shows the SAD most commonly obtained from interface regions. The square grid of diffraction spots, of which the center is marked by white lines, is the <001> zone axis pattern from melilite. The hexagonal pattern (first order spots denoted with arrows) is from UNK and corresponds to the <0001> zone axis pattern of the reciprocal lattice determined later. On the basis of the unit cell proposed below for UNK, the epitaxial relationship between

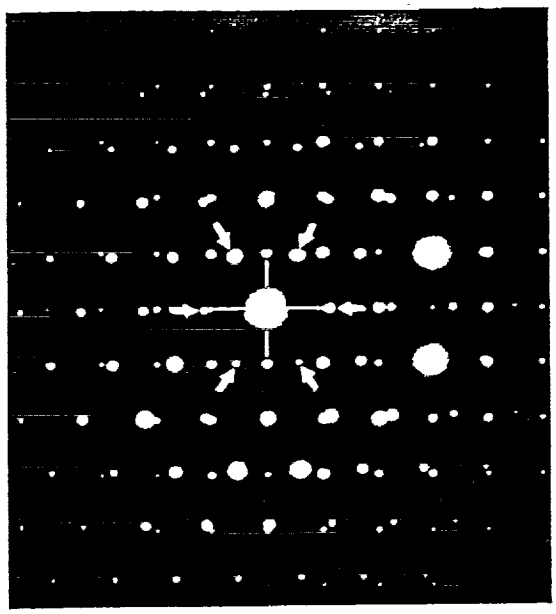

FIG. 2. Electron diffraction pattern from coherent interface between UNK and melilite, illustrating the epitaxial relationship $(0001)_{UNK} \| (001)_{mel}$ and $<10\bar{1}0>_{UNK} \| <100>_{mel}$. White lines indicate the 100-type reciprocal lattice spots from the melilite and arrows point to the $10\bar{1}0$ spots from the UNK phase. Note the three-fold symmetry.

melilite (mel) and UNK shown in Fig. 2 has the form $(001)_{mel} \| (0001)_{UNK}$, $<10\bar{1}0>_{UNK} \| <100>_{mel}$, the latter implying one pair of directions only. Examination of other major zone axis patterns from the same UNK/melilite contacts showed that good lattice matching occurred only for this orientation.

The TEM also reveals the detailed form of intergrowths with other minerals. Skeletal intergrowths of UNK and Ti-fassaite occur on the peripheries of some UNK crystals (see Fig. 7c of Paque *et al.*, 1994), and an example of this microstructure is shown in Fig. 3. Microanalysis by ATEM of these intergrown regions, obtained with the electron beam spread to a large diameter compared with the scale of the microstructure, invariably gives average compositions low in Ti and Ca, and high in Si and Mg (typically 2.4 wt% MgO, 18.1 wt% Al_2O_3, 53.0 wt% SiO_2, 24.4 wt% CaO and 2.1 wt% TiO_2) relative to bulk UNK. Moiré fringes occur at many of the convoluted interfaces, confirming that the intergrowths are semi-coherent, although microscopic twinning in the UNK is also in evidence and indicative of the strains resulting from that partial coherence. To relieve the misfit at the boundaries between UNK and the cellular microstructure, there are commonly arrays of roughly equi-spaced dislocations; members of such an array are indicated by arrows in Fig. 3

Nature of the Unit Cell

The initial approach to finding a unit cell for UNK by TEM was to use the electron diffraction mode and search reciprocal space for diffraction patterns that might correspond to major zone axes. This technique was easy when working with regions of the crystals thick enough to give Kikuchi patterns by tilting so as to progress along the Kikuchi band corresponding to the chosen row of diffraction spots. Crystals in several specimens were examined in this way so that a major fraction of UNK reciprocal space was sampled, resulting in an ordered list of reciprocal lattice spacings.

FIG. 3. Bright field image of the interface region between UNK and intergrowth of fassaite and UNK, labeled INTERGR. Arrows point to dislocations at the interface.

It was evident that at least two zone axes of high symmetry had been encountered. One of these gave a diffraction pattern with three-fold rotational symmetry, which was, in fact, the three-fold pattern from the UNK phase already illustrated in Fig. 2. We inferred from this observation that there should be another major zone axis at 90° to the triad.

The next step was to obtain a CBED pattern corresponding to the three-fold axis in order to measure the radius of the first order Laue zone (FOLZ) ring. Its radius gives approximately the spacing of crystal planes in the direction of the zone axis along which the electron beam is directed according to the equation (*e.g.*, Champness, 1987)

$$R = \sqrt{\frac{2H}{\lambda}}$$

where λ is the appropriate electron wavelength and H is the spacing of the crystallographic planes. The measured radius was calibrated in terms of the distance in reciprocal space from the undiffracted electron beam to a first order diffraction spot and converted *via* an appropriate instrumental camera factor. As mentioned earlier, CBED patterns from UNK were generally of poor quality, and although the FOLZ ring appeared weakly and without useful detail, its radius was still measurable. The result indicated that spacing of the lattice planes in the direction of the three-fold axis was about 0.5 nm. An interplanar spacing of about 0.5 nm was present in the list of observed spacings, but it had been obtained from another UNK specimen and could not immediately be established as fundamental to the diffraction pattern from a zone axis orthogonal to the assumed c-axis. However, in due course, an additional UNK crystal was obtained with a fortuitous positioning of the hypothesized c-axis with respect to the plane of the specimen. By suitably orientating this specimen in the goniometer stage with respect to the tilt axes, it was arranged that the three-fold diffraction pattern was obtained when the specimen was rolled by ~45° about the "pencil" axis of the goniometer. By then rolling in the opposite sense and making only small adjustments (<5°) to the other tilt axis (as already mentioned, this tilt axis did not give reproducible scale readings), the three-fold diffraction pattern could be related to another zone axis SAD of two-fold symmetry, which clearly corresponded to an axis at 90° to the triad.

During the operations just described, it was a simple matter to record other zone axis patterns *en route* and the settings of the goniometer stage at which they occurred. Subsequent direct use of the settings of the stage tilt angles at which the zone axis patterns occurred made possible the provisional indexing of all the low index reflections in the diffraction patterns. A reasonably accurate provisional stereographic projection was generated in this way and the approximate dimensions of the hexagonal prism-shaped reciprocal lattice cell were calculated. The latter gave provisional values for the lengths of the **c** and **a** axes of a tentative unit cell for UNK. These values and the assumption of a hexagonal-structured crystal were used as input for a computer program that calculates the spacings of lattice planes, interplanar angles, and reciprocal lattice vectors in all possible zones for a selected microscope camera constant. The data thus generated gave reasonable agreement with values derived directly from the SADs. The good agreement established that the unit cell of the reciprocal lattice could be referred to hexagonal axes with $\mathbf{c} \sim 0.5$ nm and $\mathbf{a} \sim 0.8$ nm. Figure 4 shows several SADs indexed according to this cell. It remained to measure the cell parameters more accurately and, if possible, to ascertain the full symmetry of UNK, which could be either hexagonal or trigonal based on the above data.

Each diffraction disk in a CBED pattern should ideally exhibit a rich pattern of lines caused by high order Laue zone reflections (HOLZ). Such fine structure is missing in the diffraction disks from the melt-derived UNK, which could imply the presence of strain, or high defect densities, or some disorder. Although CBED studies of CAI-type UNK were not generally satisfactory, acceptable diffraction patterns containing reflections from both the zeroth order Laue zone (ZOLZ) and FOLZ were obtainable with the electron beam parallel to several major zone axes. Diffraction spots in the FOLZ for the three-fold axis, and for axes orthogonal to it, occurred in positions that superposed when the ZOLZ reciprocal lattice layer was extended to meet the FOLZ. This implies that points of the reciprocal lattice in successive lattice layers lie immediately above one another and that no points occur at intermediate (fractional) positions with respect to lattice points in the zeroth layer. These patterns give important confirmation of the simple primitive nature of the UNK unit cell. Moreover, since the spacings of the spots in the two Laue zones were the same, there was no masking of forbidden reflections in the diffraction patterns by double diffraction effects, thereby making interpretation of the diffraction data in terms of a unit cell of the reciprocal lattice very straightforward.

Determination of Accurate Unit Cell Parameters

To overcome hysteresis in the tilt axis of the goniometer stage mentioned earlier, it was necessary to use crystals of UNK in which

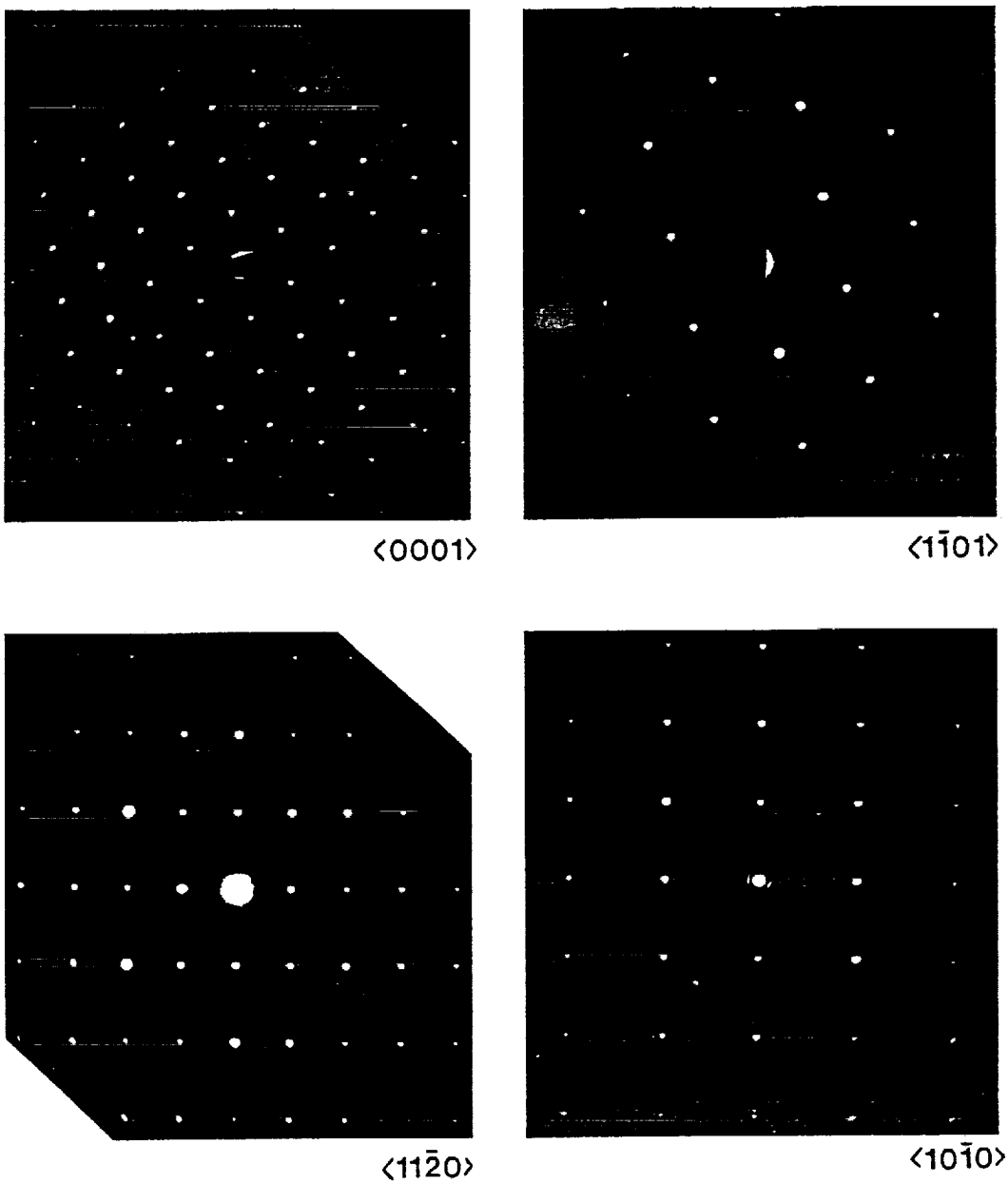

FIG. 4. Selected area electron diffraction patterns corresponding to major zone axes of UNK, indexed in terms of a hexagonal reciprocal lattice and a primitive real-space lattice.

at least two major zone axes could be accessed merely by rotation about the "pencil" axis. In principle, this would be sufficient to establish the three-dimensional geometry of the reciprocal cell with reasonable accuracy. The approach, however, required suitable crystals to be found and mounted in the stage in just the right orientation for the chosen single roll axis to be effective, a tedious and exacting procedure.

The reciprocal lattice vectors in SADs for the <0001> and <11$\bar{2}$0> zone axes, recorded from the same area of an UNK crystal, were provided with a built-in calibration by coating the specimen with a thin layer of Au and then finding a small area that had previously been X-ray microanalyzed (Fig. 5). The lattice parameters that follow apply to UNK with a wt% oxide composition of MgO ~ 0.4, Al_2O_3 ~ 19.7, SiO_2 ~ 28.7, CaO ~ 30.8, TiO_2 ~ 20.4. Care was taken to ensure that the diffraction patterns were recorded with the electron beam exactly parallel to a <11$\bar{2}$0> zone axis, since failure to do this would have affected the accuracy of the results. The 200 interplanar spacing of Au (0.2039 nm) was used as an internal calibration standard *via* the spacings of diffraction spots in the <0001> and <10$\bar{1}$0> reciprocal lattice directions because the 111_{AU} ring is very close to the UNK 30$\bar{3}$0 reflections. This causes the Au peaks to partially superpose on those of the 30$\bar{3}$0 and $\bar{3}$030 diffraction spots in microdensitometer recordings. The lattice parameters thus determined are **c** = 0.492 nm and **a** = 0.790 nm, both with an estimated accuracy of ±0.002 nm. The cell parameters are within error of values determined by

Barber and Agrell (1994) for UNK in a mixer furnace slag (**a** = 0.791 nm, **c** = 0.492 nm) and very similar to those of melilite (tetragonal with **c** = 0.50 nm and **a** = 0.78 nm for Ak_{50} melilite; Kimata, 1980) though the crystal systems are different. The **c**/**a** ratio is 0.624, and the cell volume is 0.267 nm³. For UNK of the composition given above and a unit cell containing 14 oxygens, the density is 3.34 g/cm³, comparable to that of CAI fassaites. Table 1 gives the list of measured electron diffraction spacings for low index planes together with calculated values based on the calibrated d-spacings for the (0001) and (10$\bar{1}$0) planes.

Lattice Images

Although the atom-milled UNK grains did not give particularly good high resolution images, it was possible to obtain lattice images with the electron beam parallel to both the <0001> and <11$\bar{2}$0> directions. Typical examples are illustrated in Fig. 6. The spacing of lattice fringes in these images is consistent with the interplanar spacings (Table 1) derived from diffraction patterns for the zone axis orientations and supports the conclusions concerning the primitive nature of the unit cell and its dimensions. No defects are visible in the lattice images (conventional SADs are not sensitive to a low density of crystal defects). Nor are there other features that explain the lack of fine structure in HOLZ patterns, which might therefore be due partly to preparation procedures.

DISCUSSION

Structure of UNK

Each mineral in a CAI carries within it information that can be used to constrain the origin and evolution of the host inclusion and, hence, of the early history of the Solar System. While it is certainly possible to obtain useful information on the nebular environment in a strictly empirical fashion, an understanding of the stability of solid solutions such as UNK or of trace element partitioning between UNK and melt ± vapor ± other crystals requires some understanding of the crystal structure and crystal chemistry of the phase (*e.g.*, Beckett, *et al.*, 1990; Beckett and Stolper, 1994). In this section, we explore constraints on the crystal structure of UNK imposed by stoichiometry, chemical variability, cell parameters, and allowable space groups. We then consider implications of the UNK structure for equilibria involving other minerals.

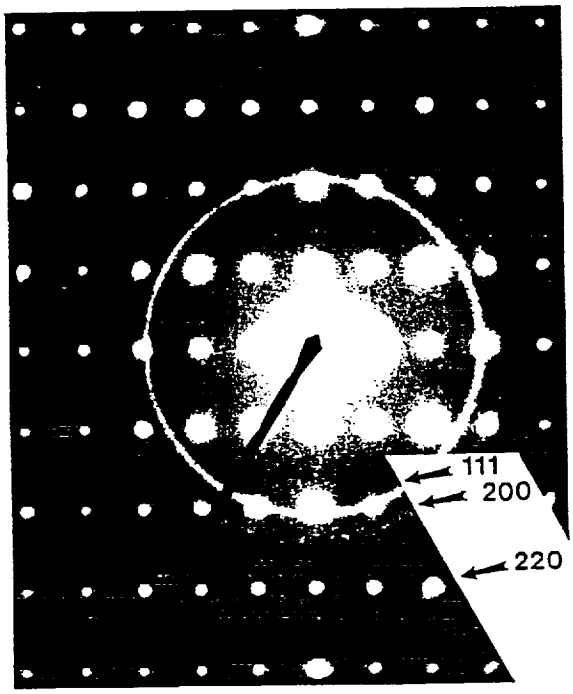

Fig. 5. Electron diffraction pattern for the <10$\bar{1}$0> zone axis of UNK with superposed (111), (200) and (220) rings from evaporated Au film.

Paque *et al.* (1994) describe the composition of synthetic and meteoritic UNK in some detail. The UNK has 3.0 cations of Ca in a formula unit based on 14 oxygens. Choosing an alternative formula unit leads either to a non-integer number of Ca or to anomalously high densities (*e.g.*, a formula unit based on 28 oxygens results in a theoretical density of 6.7 g/cm³). Provided there are 14 oxygens and three Ca cations in the formula unit, the Ti, Al and Si must (for available analyses) be distributed among six

TABLE 1. Interplanar spacings (averaged) measured from electron diffraction patterns and calculated spacings for hexagonal unit cell

Plane (hkil)	Interplanar spacing (measured: nm)	Reciprocal spacing (calculated: nm)
01$\bar{1}$0	0.6840 *	5.374
0001	0.4909	7.464
01$\bar{1}$1	0.4004	9.198
11$\bar{2}$0	0.3937	9.309
02$\bar{2}$0	0.3431	10.749
11$\bar{2}$1	0.3043	11.932
02$\bar{2}$1	0.2783	13.086
12$\bar{3}$0	0.2589	14.219
0002	0.2459	14.928
01$\bar{1}$2	0.2313	15.866
12$\bar{3}$1	0.2291	16.059
03$\bar{3}$0	0.2277	16.123
11$\bar{2}$2	0.2079	17.592
03$\bar{3}$1	0.2061	17.767
02$\bar{2}$2	0.2005	18.395
22$\bar{4}$0	0.1976	18.617
13$\bar{4}$0	-	19.378
22$\bar{4}$1	-	20.058
12$\bar{3}$2	-	20.616
13$\bar{4}$1	-	20.765
04$\bar{4}$0	-	21.497
03$\bar{3}$2	0.1669	21.973
0003	0.1642	22.392
04$\bar{4}$1	-	22.756
01$\bar{1}$3	0.1593	23.028
23$\bar{5}$0	-	23.426
22$\bar{4}$2	-	23.863
11$\bar{2}$3	-	23.250
13$\bar{4}$2	-	24.461
13$\bar{4}$2	0.1502	24.587
14$\bar{5}$0	-	24.628
02$\bar{2}$3	0.1473	24.838
30$\bar{3}$3	0.1325	27.593
10$\bar{1}$4	0.1204	30.336

* Calibrated in terms of the Au(200)spacing and used to determine the UNK lattice parameters from which the data in column 3 are calculated.

sites with 2.2–2.5 cations of Si, 1.8–2.1 cations of Al and 1.3–1.9 cations of Ti. Silicon is almost certainly located exclusively in tetrahedral sites, so there must be at least three tetrahedra/formula unit in order to accomodate the >2 cations of Si. Paque *et al.* (1994) were able to synthesize a Ti-free analog of UNK with a formula of $Ca_3Al_2Si_4O_{14}$. There is a large gap in composition between this phase and the Ti-bearing UNK crystals described here and in Barber and Agrell (1994) so the structures may also be different. Nevertheless, the existence of $Ca_3Al_2Si_4O_{14}$, which must contain at least four tetrahedral sites, suggests that there may also be four or more tetrahedral sites in the unit cell of UNK. Based solely on chemistry, the substitution mechanism for Ti is unclear as either direct substitutions for Si or coupled substitutions involving Si and Al are possible. Moreover, Al and Ti are known to substitute into four-, five- or six-coordinated sites (Moore and Louisnathan, 1967; Waychunas, 1987; Kerrick, 1990; Della Ventura *et al.*, 1991) although Ti prefers octahedral coordination, so all three possibilities must be considered.

The striking similarity of the cell parameters of UNK and melilite together with the tendency for UNK to grow epitaxially on the (001) and (100) faces of melilite suggests that there are also similarities in the two structures even though they crystallize in different systems. The structure of melilite can be described as a puckered sheet of tetrahedra perpendicular to the c-direction coordinated by near-planar layers of Ca (Louisnathan, 1971). In general, crystals with primitive space groups tend to be layer structures so it is reasonable to hypothesize that the structure of UNK, which has no center of symmetry (Barber and Agrell, 1994), involves sheets of Al-, Si-, Ti-centered polyhedra coordinated by sheets of Ca.

Barber and Agrell (1994) were able to constrain the space group of UNK from a mixer furnace slag to being either P31m or P3ml. In both space groups, a general position has a multiplicity of six. Special positions in mirror planes generate three equivalent positions/unit cell, and those along three-fold axes have a multiplicity of one or two. Each of the 14 oxygens in the unit cell must be coordinated to one or more polyhedra containing Al, Si, and/or Ti and all of the oxygens in the structure can be accounted for in terms of six of these polyhedra/unit cell. At least three of the polyhedra are tetrahedra, but the remaining three Al +Ti + Si sites may, in principle, be four-, five- or six- coordinated with O. The combination of stoichiometry constraints and the two allowable space groups, however, greatly restricts the possible structure of UNK. For example, if the structure contained four tetrahedra and two octahedra, three of the tetrahedra would have to be centered in mirror planes while the two octahedrally and one of the tetrahedrally coordinated cations would lie along three-fold axes. Unless shared tetrahedral edges are allowed, there would be at least one unshared vertex corresponding to the apical O of the unique tetrahedron. However, four tetrahedra and two octahedra have a total of 4 x 4 + 2 x 6 = 28 vertices and, upon introducing the stoichiometric constraint of 14 oxygens/unit cell, there must be 28–14 = 14 shared vertices (*i.e.*, all vertices are shared). This contradicts the requirement that there be at least one unshared vertex, so the class of structures involving four tetrahedra and two octahedra can be rejected. Similar arguments can be used to reject all classes of possible UNK structures except those that place Ca and three of the tetrahedrally coordinated cations in mirror planes and one octahedrally and two tetrahedrally coordinated cations along the three-fold axes.

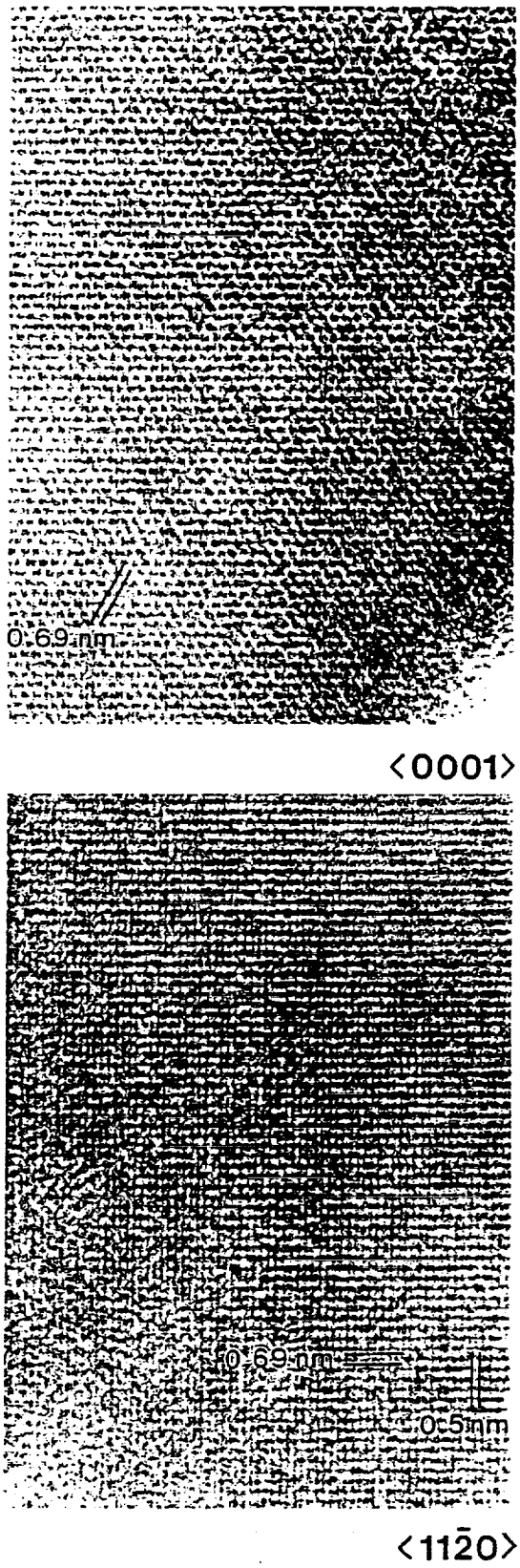

FIG. 6. Lattice images of UNK recorded with the electron beam parallel to (a) <0001> and (b) <11$\bar{2}$0>.

Based on the above discussion, the structural formula of UNK has the form

$$Ca_3^{VIII}X^{VI}Y_2^{IV}Z_3^{IV}O_{14}.$$

The X-site is most likely occupied almost completely by Ti because there is always more than one Ti^{4+}/formula unit in UNK analyzed by Paque *et al.* (1994), and Ti generally greatly prefers octahedral coordination in silicates. Constraints on site assignments for the remaining cations are ambiguous. We assume that the Y sites are occupied mostly by Al and Ti and the Z sites mostly by Si because this places Ti and Si on different crystallographic sites; we also recognize that alternative site assignments are possible. To a good approximation, the compositions of meteoritic and synthetic Ti-bearing UNK (Paque *et al.*, 1994) can then be described as a binary solid solution between the end-members

$$Ca_3^{VIII}Ti^{VI}Al_2^{IV}Si_3^{IV}O_{14} \text{ and } Ca_3^{VIII}Ti^{VI}(AlTi)^{IV}(AlSi_2)^{IV}O_{14}.$$

Small amounts of Ti^{3+} that may be present in meteoritic UNK (Paque *et al.*, 1994) probably substitute into the octahedral site, again due to the strong preference of Ti for octahedral coordination. Paque *et al.* (1994) also analyzed a Ti-free phase for which we infer a formula based on 14 oxygens of

$$Ca_3^{VIII}Al^{VI}(AlSi)^{V}(Si)_3^{IV}O_{14}.$$

This phase is plausibly related structurally to Ti-bearing UNK with the octahedral site being completely occupied by Al.

Origin of UNK in Calcium- Aluminum-rich Inclusions

Meteoritic UNK occurs exclusively within melilite as monomineralic inclusions. There are three classes of models for the origin of UNK (Allen *et al.*, 1978; Paque *et al.*, 1986, 1994) all of which we consider below. These involve alteration, exsolution, and crystallization from a melt.

Titanium does not appear to have been very mobile during low-temperature alteration of CAIs. Most of the Ti occurs in phases such as fassaite, perovskite and hibonite that are quite resistant to the process (*e.g.*, Allen *et al.*, 1978; Barber *et al.*, 1984) although ilmenite lining margins of, and cracks within, perovskite and fassaite is occasionally observed (Kornacki and Wood, 1985; Hashimoto and Grossman, 1987). Thus, if UNK formed either as an exsolution or alteration product of melilite, then melilite itself was probably the source of the Ti. The precise nature of such an UNK-forming reaction would depend, however, on the mechanism of Ti substitution into melilite, for which there are few constraints. For illustrative purposes, we assume that the ~100 ppm Ti in CAI melilite (Johnson *et al.*, 1988) substitutes either into the Ca-site accomodated by a defect molecule of the form $CaTi\square Si_2O_7$, where $\square$ refers to a vacant Mg-Al site, or into interstitial sites,

$$Ti_{(mel)}^{interstitial},$$

charge-balanced by Si vacancies. Simple reactions between melilite and UNK can then be written

$$CaTi\square Si_2O_{7\,(mel)} + Ca_2Al_2SiO_{7\,(mel)} = Ca_3TiAl_2Si_3O_{14\,(UNK)} \quad \text{Equ. (1)}$$

or

$$Ti_{(mel)}^{interstitial} + Ca_3TiAl_2Si_3O_{14\,(UNK)} = Si_{(mel)}^{IV} + Ca_3Ti_2Al_2Si_2O_{14\,(UNK)}. \quad \text{Equ.(2)}$$

Reaction (1) could involve either exsolution from the melilite lattice or, perhaps more likely, nucleation on the abundant dislocations (Barber *et al.*, 1984) that characterize CAI melilites. Note that gehlenitic melilite is consumed in reaction (1) and that UNK is nearly Mg-free. This could account for observed enrichments of Mg near the interface between meteoritic UNK and host melilite (Paque *et al.*, 1994). Alternatively, since Si, Mg and Ca were all mobile, probably as hydroxide species, during low temperature alteration of CAIs (Hashimoto, 1992), reactions to form UNK may have been balanced by various combinations of Mg, Ca and/or Si species in the vapor. It is expected that if UNK formed by either exsolution from melilite or alteration processes, then trace element abundances would be relatively low, consistent with abundances in the host melilite.

UNK is readily produced in cooling rate experiments on partially molten samples with bulk compositions corresponding to those of CAIs so we know that crystallization of meteoritic UNK from a melt is at least possible. Moreover, UNK in the unique Essebi inclusion described by El Goresy *et al.* (1984) is enriched in Hf and the rare earth elements (REE) consistent with crystallization from a late-stage residual melt. There are, however, two difficulties with such a model for most UNK from CAIs. First, in experiments discussed by Paque *et al.* (1994), UNK is a very late-stage crystallization product, whereas in CAIs, UNK usually occurs in texturally early melilite. Second, although it is possible to find in the experimental run products examples of UNK + melilite with no other associated phases, other phases are often present. In meteoritic occurrences, such additional phases are not found, which argues against, for example, the possibility that UNK crystallized from melt inclusions trapped within early crystallizing melilite. Neither of these two major objections necessarily rules out crystallization from a melt. Small pyroxene inclusions that have trace element abundances consistent with very late stage crystallization from a melt are often observed in texturally early CAI melilite from the mantles of B1 inclusions (Simon *et al.*, 1991) and texturally similar occurrences are observed in experimental run-products (MacPherson *et al.*, 1984). It is also worth noting that Mg is often enriched in the melilite adjacent to the natural pyroxene inclusions and adjacent to UNK formed experimentally by crystallization of CAI-like bulk compositions. This feature is also observed in the vicinity of meteoritic UNK.

At present, we can not reject any of the three proposed models for the origin of UNK in CAIs. However, trace element abundances should provide less ambiguous constraints. If meteoritic UNK exsolved from melilite or formed during the alteration process, then many trace elements will not be strongly enriched because the host melilite has relatively low abundances. On the other hand, UNK that crystallized from a late stage melt should be strongly enriched even in very incompatible trace elements, a reflection of trace element abundances in the melt. As noted above, one meteoritic occurrence of UNK is known to exhibit such trace element enrichments (El Goresy *et al.*, 1984) but the host inclusion is so unusual that it is not possible to make inferences based on it about the UNK occurrences described here.

CONCLUSIONS

UNK has a primitive hexagonal or trigonal unit cell with cell parameters, $a = 0.790 \pm 0.002$ nm and $c = 0.492 \pm 0.002$ nm, similar to those of melilite (tetragonal with $a = 0.78$ nm, $c = 0.50$ nm for Ak_{50}; Kimata, 1980). It frequently displays an epitactic

relationship in which melilite acts as the host, with $(0001)_{UNK} \parallel (001)_{mel}$ and $<10\bar{1}0>_{UNK} \parallel <100>_{mel}$. The observed epitaxial relationship and the similarity of the cell parameters to those of melilite suggest that the structure may be related to that of intermediate melilites on the åkermanite-gehlenite join, but that the presence of Ti and absence of Mg induces a different symmetry. The results presented in Barber and Agrell (1994) show that the space group of UNK is restricted to one of P3m1 or P31m. It is testimony to the organization, memory and perception of the second author of that paper that a phase discovered through applied mineralogy during World War II (Agrell, 1945) should be so instrumental in research half a century later. Only with constraints on the space group obtained from Agrell's sample do other crystallographic, stoichiometric and chemical constraints developed in Paque *et al.* (1994) and in this study lead to a basic understanding of the crystal chemistry of UNK. The structure probably consists of puckered sheets of tetrahedra and octahedra coordinated by sheets of Ca. The proposed structural formula is

$$Ca_3^{VIII}(Ti,Al)^{VI}(Al,Si,Ti)_2^{IV}(Si,Al)_3^{IV}O_{14}$$

where Si + Ti = 4, and the compositions of meteoritic and synthetic Ti-bearing examples can be described mostly as a binary solid solution between the end-members $Ca_3TiAl_2Si_3O_{14}$ and $Ca_3Ti(AlTi)(AlSi_2)O_{14}$ with small amounts of trivalent Ti substituting in some cases for Al^{VI}. A Ti-free analog synthesized by Paque *et al.* (1994) is probably related structurally to Ti-bearing UNK with the octahedral site being completely occupied by Al; that is

$$Ca_3^{VIII}Al^{VI}(AlSi)^{IV}(Si)_3^{IV}O_{14}\ .$$

Meteoritic UNK may have crystallized from melts, exsolved from melilite or formed during alteration of the host CAI. Measurement of trace element abundances of UNK should provide strong constraints on the mode of origin for this phase.

Acknowledgments—The role of Ian Hutcheon in acting as an initial liaison for the authors is greatly appreciated. DJB wishes to thank Prof. W. F. Müller for his kind hospitality and for access to the CM12 microscope at the Technische Hochschule Darmstadt, Germany. All of the authors acknowledge the helpful comments of A. Brearley and an anonymous reviewer. This work was supported by NASA grants NAG9-105 and NAGW-3533, NERC grant GR3/5349 and SETI grant NCC 2-758. Caltech Division of Geological and Planetary Sciences, Division Contribution No. 5137.

Editorial handling: K. Keil

REFERENCES

AGRELL S. O. (1945) Mineralogical observations on some basic open-hearth slags. *J. Iron Steel Inst. Lond.* **152**, 19P–55P.

ALLEN J. M., GROSSMAN L., DAVIS A. M. AND HUTCHEON I. D. (1978) Mineralogy, textures and mode of formation of a hibonite-bearing Allende inclusion. *Proc. Lunar Planet. Sci. Conf.* **9th**, 1209–1233.

BARBER D. J. AND AGRELL S. O. (1994) A new titanium-bearing calcium aluminosilicate phase: III. Crystals from a mixer furnace slag. *Meteoritics* **29**, 691–695.

BARBER D. J., MARTIN P. M. AND HUTCHEON I. D. (1984) The microstructure of minerals in coarse-grained Ca-Al-rich inclusions from the Allende meteorite. *Geochim. Cosmochim. Acta* **48**, 769–783.

BECKETT J. R. AND STOLPER E. (1994) The stability of hibonite, melilite and other aluminous phases in silicate melts: Implications for the origin of hibonite-bearing inclusions from carbonaceous chondrites. *Meteoritics* **29**, 41–65.

BECKETT J. R., SPIVACK A. J., HUTCHEON I. D., WASSERBURG G. J. AND STOLPER E. (1990) Crystal chemical effects on the partitioning of trace elements between mineral and melt: An experimental study of melilite with applications to refractory inclusions from carbonaceous chondrites. *Geochim. Cosmochim. Acta* **54**, 1755–1774.

CHAMPNESS P. E. (1987) Convergent beam electron diffraction. *Mineral. Mag.* **51**, 33–48.

CLIFF G. AND LORIMER G. W. (1975) The quantitative analysis of thin specimens. *J. Microscopy* **103**, 203–207.

DELLA VENTURA G., ROBERT J.-L. AND BÉNY J.-M. (1991) Tetrahedrally coordinated Ti^{4+} in synthetic Ti-rich potassic richterite: Evidence from XRD, FTIR, and Raman studies. *Am. Mineral.* **76**, 1134–1140.

EL GORESY A., PALME H., YABUKI H., NAGEL K., HERRWERTH I. AND RAMDOHR P. (1984) A calcium-aluminum-rich inclusion from the Essebi (CM2) chondrite: Evidence for captured spinel-hibonite spherules and for an ultra-refractory rimming sequence. *Geochim. Cosmochim. Acta* **48**, 2283–2298.

FLOSS C., EL GORESY A., PALME H., SPETTEL B. AND ZINNER E. (1992) An unusual Ca-Ti-Al silicate in a Type A Allende inclusion (abstract). *Meteoritics* **27**, 220.

FUCHS L. H. (1978) The mineralogy of rhönite-bearing calcium aluminum rich inclusion in the Allende meteorite. *Meteoritics* **13**, 73–88.

GOODMAN P. (1980) Setting up convergent beam electron diffraction for materials analysis using a TEM. In *Scanning Electron Microscopy, Vol. I* (ed. O. Johari), pp. 53–60. SEM, AMF O'Hare, Chicago, Illinois.

GROSSMAN L. (1975) Petrography and mineral chemistry of Ca-rich inclusions in the Allende meteorite. *Geochim. Cosmochim. Acta* **39**, 433–454.

GROSSMAN L. (1980) Refractory inclusions in the Allende meteorite. *Ann. Rev. Earth Planet. Sci.* **8**, 559–608.

HASHIMOTO A. (1992) The effect of H_2O gas on volatilities of planet-forming elements: I. Experimental determination of thermodynamic properties of Ca-, Al-, and Si-hydroxide gas molecules and its application to the solar nebula. *Geochim. Cosmochim. Acta* **56**, 511–532.

HASHIMOTO A. AND GROSSMAN L. (1987) Alteration of Al-rich inclusions inside amoeboid olivine aggregates in the Allende meteorite. *Geochim. Cosmochim. Acta* **51**, 1685–1704.

JOHNSON M. L., BURNETT D. S. AND WOOLUM D. S. (1988) Relict refractory element rich phases in Type B CAI (abstract). *Meteoritics* **23**, 276.

KERRICK D. M. (1990) The Al_2SiO_5 polymorphs. *Rev. Mineral.* **22**, 1–406.

KIMATA M. (1980) Crystal chemistry of Ca-melilites on X-ray diffraction and inferred absorption properties. *N. Jb. Miner. Abh.* **139**, 43–58.

KORNACKI A. S. AND WOOD J. A. (1985) Mineral chemistry and origin of spinel-rich inclusions in the Allende CV3 chondrite *Geochim. Cosmochim. Acta* **49**, 1219–1237.

LOUISNATHAN J. S. (1971) Refinement of the crystal structure of a natural gehlenite, $Ca_2Al(Al,Si)_2O_7$. *Can. Mineral.* **10**, 822–837.

MACPHERSON G. J., PAQUE J. M., STOLPER E. AND GROSSMAN L. (1984) The origin and significance of reverse zoning in melilite from Allende Type B inclusions. *J. Geol.* **92**, 289–305.

MACPHERSON G. J., WARK D. A. AND ARMSTRONG J. T. (1988) Primitive material surviving in chondrites: Refractory inclusions. In *Meteorites and the Early Solar System* (eds. J. F. Kerridge and M. S. Mathews), pp. 746–807. Univ. Arizona Press, Tucson, Arizona.

MOORE P. B. AND LOUISNATHAN J. (1967) Fresnoite: Unusual titanium coordination. *Science* **156**, 1361–1362.

PAQUE J. M. AND STOLPER E. (1984) Crystallization experiments on a range of Ca-Al-rich inclusion compositions (abstract). *Lunar Planet. Sci.* **15**, 631–632.

PAQUE J. M., BECKETT J. R. AND STOLPER E. (1986) A new Ca-Al-Ti silicate in coarse-grained Ca-Al-rich inclusions (abstract). *Lunar Planet. Sci.* **17**, 646–647.

PAQUE J. M., BECKETT J. R., BARBER D. J. AND STOLPER E. (1994), A new titanium-bearing calcium aluminosilicate phase: I. Meteoritic occurrences and formation in synthetic systems. *Meteoritics* **29**, 673–682.

SIMON S. B., GROSSMAN L. AND DAVIS A. M. (1991) Fassaite composition trends during crystallization of Allende Type B refractory inclusion melts. *Geochim. Cosmochim. Acta* **55**, 2635–2656.

STEEDS J. W. (1979) Convergent beam electron diffraction. In *Introduction to Analytical Electron Microscopy* (eds. J. J. Hren, J. I. Goldstein and D. C. Joy), pp. 387–422. Plenum Press, New York, New York.

STOLPER E. AND PAQUE J. M. (1986) Crystallization sequences of Ca-Al-rich inclusions from Allende: The effects of cooling rate and maximum temperature. *Geochim. Cosmochim. Acta* **50**, 1785–1806.

WAYCHUNAS G. A. (1987) Synchrotron radiation XANES spectroscopy of Ti in minerals: Effects of Ti bonding distances, Ti valence, and site geometry on absorption edge structure. *Am. Mineral.* **72**, 89–101.

WILLIAMS D. B. (1984) *Practical Analytical Electron Microscopy in Materials Science.* Philips Electronic Instruments, Inc., Electron Optics Publishing Group, Einhoven, The Netherlands.